

# Freestanding Perovskite Oxide Films

## Synthesis, Challenges, and Properties

**Chiabrera, Francesco M.; Yun, Shinhee; Li, Ying; Dahm, Rasmus T.; Zhang, Haiwu; Kirchert, Charline K. R.; Christensen, Dennis V.; Trier, Felix; Jespersen, Thomas S.; Pryds, Nini**

*Published in:*
Annalen der Physik

*Link to article, DOI:*
10.1002/andp.202200084

*Publication date:*
2022

*Document Version*
Publisher's PDF, also known as Version of record

annalen der physik
www.ann-phys.org

# Freestanding Perovskite Oxide Films: Synthesis, Challenges, and Properties

*Francesco M. Chiabrera, Shinhee Yun, Ying Li, Rasmus T. Dahm, Haiwu Zhang, Charline K. R. Kirchert, Dennis V. Christensen, Felix Trier, Thomas S. Jespersen, and Nini Pryds**

**In this review paper, recent progress in the fabrication, transfer, and fundamental physical properties of freestanding oxide perovskite thin films is discussed. First, the main strategies for the synthesis and transfer of freestanding perovskite thin films are analyzed. In this initial section, particular attention is devoted to the use of water-soluble $(Ca,Sr,Ba)_3Al_2O_6$ thin films as sacrificial layers, one of the most promising techniques for the fabrication of perovskite membranes. The main functionalities that have been observed in freestanding perovskite thin films are then reviewed. In doing so, the authors begin by describing the emergence of new phenomena in ultrathin perovskite membranes when released from the substrate. They then move on to a summary of the functional properties that are observed in freestanding perovskite membranes under the application of strain. Indeed, freestanding thin films offer the unique possibility to actively control the strain state far beyond what can be observed with traditional methods, allowing the investigation of the profound interplay between structural and electronic properties in oxides. Overall, this review highlights the potential of oxide-based freestanding thin films to become the preferred platform for the study of novel functionalities in perovskite oxide materials.**

## 1. Introduction

In December of 1959 Richard Feynman proposed in his famous lecture "There's Plenty of Room at the Bottom" that layered heterostructures could host properties and phenomena not present in the constituent materials alone.[1] Nearly 63 years later this statement is still relevant. After decades of progress in the field, conventional 2D materials—such as graphene and transition-metal dichalcogenides—as well as advanced methods for the synthesis of these materials into layered structures have been widely investigated.[2,3] Despite the large number of oxides that occur in 2D layered crystal structures, ultrathin freestanding oxides were only recently identified as one of the future directions in ceramics by a recent National Science Foundation workshop.[4] Here, we review the recent progress in the fabrication, transfer, and fundamental physical properties of freestanding oxide perovskite thin films.

Transition metal oxides thin films constitute an exciting class of electronic and ionic materials with a plethora of functionalities, including superconductivity, ferro-, pyro-, and piezoelectricity, ferromagnetism, and multiferroicity.[5–7] This richness arises from a strong interaction between the charge, orbital, spin, and structural properties, which enables the realization of functional devices with functionalities beyond those possible with standard semiconductors. Perovskites represent one of the most important crystal structures among transition metal oxides.

This crystal structure has the general formula $ABO_3$ and includes an octahedron of oxygen ions surrounding each B-site cation. Materials with the perovskite structure may have a highly symmetric cubic lattice, which when distorted can induce tilting and rotation of the oxygen octahedra. The tilted and rotated octahedra may in turn dictate the dielectric, magnetic, optical, and catalytic properties of the perovskites. The properties of oxides in general, and of perovskites in particular, are closely coupled to their lattice. Breaking the lattice symmetry can therefore result in prominent changes in the material's properties. This is particularly the case when two oxides form a heterointerface, where completely different electronic and ionic properties emerge at

F. M. Chiabrera, S. Yun, Y. Li, R. T. Dahm, H. Zhang, C. K. R. Kirchert, D. V. Christensen, F. Trier, T. S. Jespersen, N. Pryds
Department of Energy Conversion and Storage
Denmark University of Technology (DTU)
Fysikvej 310, Kongens Lyngby 2800, Denmark
E-mail: nipr@dtu.dk
Y. Li
The State Key Laboratory of Refractories and Metallurgy, Collaborative Innovation Center for Advanced Steels, International Research Institute for Steel Technology, Faculty of Science
Wuhan University of Science and Technology
Wuhan 430081, China

The ORCID identification number(s) for the author(s) of this article can be found under https://doi.org/10.1002/andp.202200084



**DOI: 10.1002/andp.202200084**

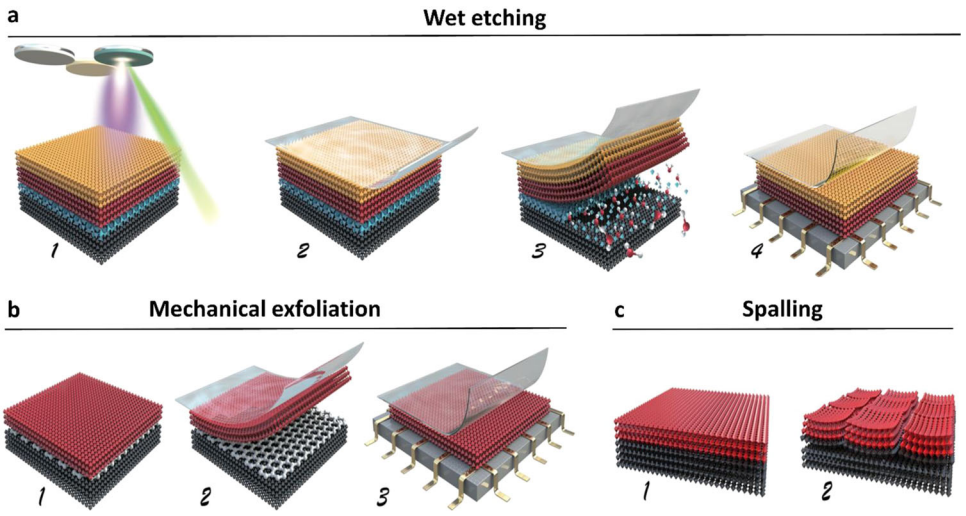


**Figure 1.** Fabrication of single-crystal free-stranding thin films, a) wet etching of sacrificial layers: 1) Deposition of the sacrificial layer and the target thin films, 2) application of a polymer on the film for easing the transfer process, 3) dissolution of the sacrificial layer with a liquid etchant, and 4) transfer of the layer onto another substrate. b) Mechanical exfoliation method: 1) Deposition of target thin film onto a 2D material, 2) cleavage of the deposited layer and 3) transfer onto another substrate. c) Self-formed freestanding thin films through spalling: 1) deposition the film (e.g., $LaAlO_3$) onto a substrate (e.g., $SrTiO_3$), and 2) forming fragmented flakes above a critical thickness.

the interface. Traditionally, these complex oxide thin-films and interfaces are grown epitaxially with a well-regulated growth scheme and atomic-level control over the material interfaces and substrate surfaces. However, these methods have fundamental limitations that prevent an unrestricted manipulation, integration, and utilization of these materials owing to the fact that:

1) Heteroepitaxy only works for a limited set of material systems with similar crystal structures, lattice orientations, and lattice parameters.
2) Epitaxial films are clamped by the substrate with the properties of the ultrathin films often affected by substrate interactions
3) During the high-temperature growth of epitaxial films, it is inevitable to have a mixture of the two layers leading to cationic interdiffusion,[8] which prevents the study of truly sharp interphases.
4) Epitaxial growth typically requires elevated temperatures, often preventing the integration of materials which are stable in different environments or which are thermodynamically unstable when in contact with each other.

Recently, new methods have been developed, bridging the realms of epitaxial complex oxides and low-dimensional van der Waals (vdW) materials systems. By replicating concepts previously developed in semiconductor technology,[9,10] the realization of freestanding perovskite films was demonstrated. Through controllable weakening of epitaxial crystals and epitaxial water-soluble sacrificial crystal layers, it is now possible to detach ultrathin complex oxide crystals (i.e., typically 50–100nm but in principle can be of any thickness above one unit cell[11]) from their substrate to realize freestanding thin films. Different strategies for fabricating freestanding layers have been demonstrated as illustrated in **Figure 1**: 1) Freestanding thin films using wet etching of sacrificial layers;[12,13] 2) Mechanical exfoliation method of epitaxial oxide crystals;[14] and 3) Self-formed freestanding thin films through spalling.[15,16] Recently, heterostructures have also been fabricated by stacking membranes directly.[14] These results demonstrate an exciting general approach for producing freestanding thin films and multilayers. The membranes can be made of functional perovskite oxides and transferred directly onto any substrate, thus bypassing the limitations of conventional epitaxy.[17] Moreover, freestanding thin films have been shown to display different functionalities when released from their substrate, thus presenting a new playground for investigating fundamental properties into large regimes of strain and strain gradients. This broadly defined field is rapidly developing and this review paper is aimed at describing the current state of the art of freestanding perovskites oxide: their synthesis, fabrication, transfer, and functional properties. Finally, the review will also provide an outlook on the current state.

## 2. Fabrication of Single-Crystal Freestanding Thin Films

In this section, the most common methods for fabricating freestanding perovskite membranes are reviewed. We will focus on the methods that allow achieving of high-quality single-crystal oxide thin films: wet etching of sacrificial layers, mechanical exfoliation of epitaxial oxide crystals, and self-formed freestanding thin films through spalling.

### 2.1. Wet Etching of Sacrificial Layers

Wet etching release/epitaxial lift-off is emerging as one of the most reliable method for obtaining high-quality single-crystal of freestanding perovskite oxides.[12,18] In this method, the perovskite oxide of interest is grown on top of a sacrificial layer which

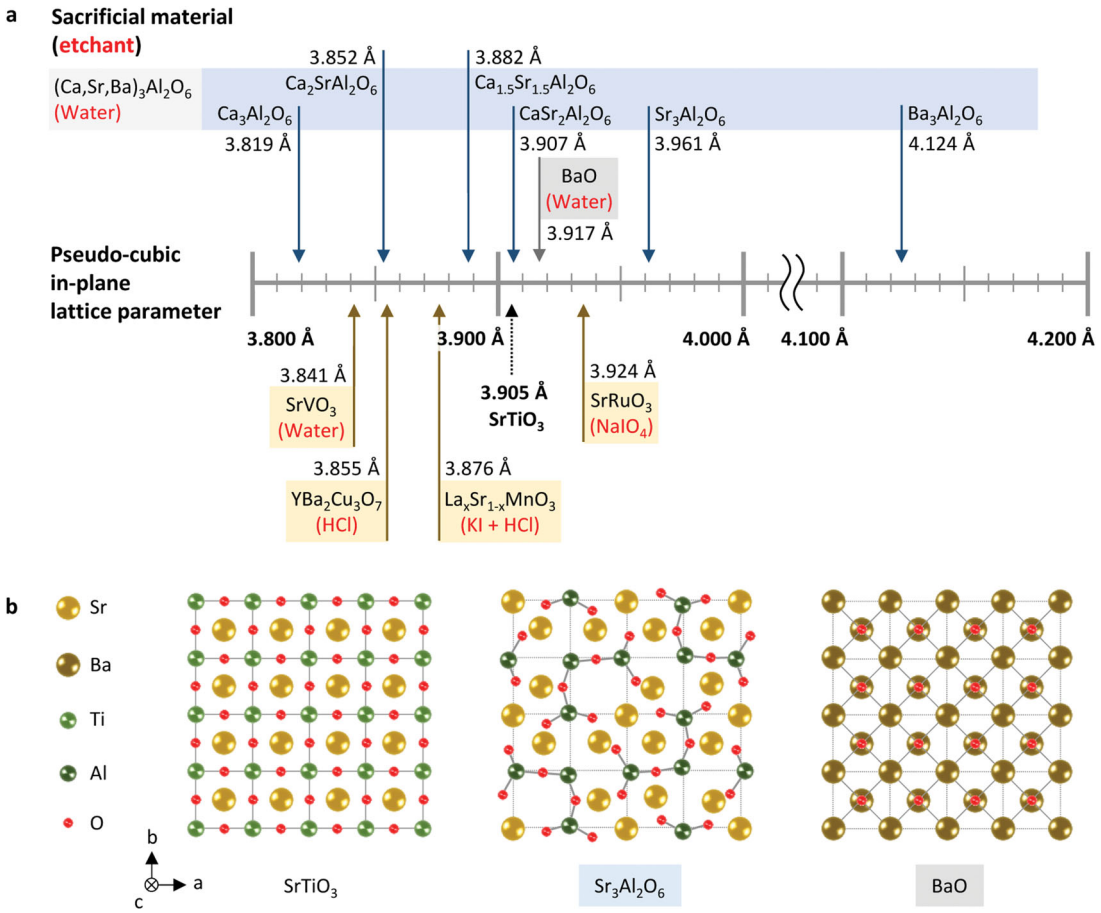


**Figure 2.** Sacrificial materials compatible with perovskite oxides. a) Pseudo-cubic in-plane lattice parameters of sacrificial materials with the representative perovskite oxide ($SrTiO_3$ indicated by a black dashed arrow). Each etchant is written in red inside parenthesis. The blue arrow represents the family of $(Ca,Sr,Ba)_3Al_2O_6$, and the brown arrow does perovskite oxide or layered perovskite oxide. The grey arrow indicates metal oxide with a rock salt structure. b) Schematic of crystal structures for $SrTiO_3$, $Sr_3Al_2O_6$, and BaO projected onto the $(001)_{pc}$ plane. Note that $SrTiO_3$, $Sr_3Al_2O_6$, and BaO are displayed as $1 \times 1$, $4 \times 4$, and $2\sqrt{2} \times 2\sqrt{2}$ unit cells, respectively.

is then dissolved by selective etching, releasing the freestanding membrane (Figure 1a). An ideal sacrificial layer should thus: 1) present a facile epitaxial growth on perovskite oxide substrates with custom orientation, 2) allow a coherent epitaxial growth of perovskite oxide films, and 3) present a high selectivity toward the liquid etchant. In the following, the main sacrificial layers proposed in the literature and the main transfer methods are reviewed.

### 2.1.1. $(Ca,Sr,Ba)_3Al_2O_6$

The family $(Ca,Sr,Ba)_3Al_2O_6$ has been largely used as sacrificial layer for growing perovskite oxides due to a facile dissolution in water and to a good structural and chemical compatibility with perovskite oxides.[12,19–23] For example, $Sr_3Al_2O_6$ (SAO) possesses a cubic unit cell (space group *Pa*3) with lattice constant equal to 15.844 Å, consisting of Sr ions and $AlO_4$ tetrahedra.[24] This structure resembles quite well four unit cells of many perovskite oxides ($a_{SAO}/4 = 3.961$ Å) and the epitaxial growth is allowed by a 75% match of the oxygen sublattice of the two structures, see **Figure 2**b. For this reason, SAO was extensively used as sacrificial layer for the growth of a variety of epitaxial perovskite thin films, as listed in **Table 1**. Using pulsed laser deposition (PLD) or molecular beam epitaxy (MBE), perovskite oxide membranes were grown on SAO in a layer-by-layer mode, attested by clear reflection high energy electron diffraction oscillations.[12,25] Structural characterizations of ultrathin membranes revealed that the crystallinity of the layers remains close to the seed films down to few unit cells.[11,26] It is worth noticing that the epitaxial relation between SAO sacrificial layers and other perovskite oxides is not limited to the (001) orientation, but also extends to other crystallographic orientations. As an example, single-crystal (110)- and (111)-oriented membranes of $SrRuO_3$ (SRO) and $La_{0.67}Sr_{0.33}MnO_3$ were successfully grown on SAO sacrificial layer and transferred onto arbitrary substrates.[27,28]

Interestingly, by controlling the ratio between Ca, Sr, and Ba the reduced lattice parameter of $(Ca,Sr,Ba)_3Al_2O_6$ can be continuously tuned from 3.819 Å (100% Ca) to 4.124 Å (100% Ba) (Figure 2a).[57,56] For example, $Ca_2SrAl_2O_6$ was used as a seed sacrificial layer for $La_{0.7}Ca_{0.3}MnO_3$ growth due to the nearly perfect lattice match (<0.1%).[55] The minimization lattice mismatches

**Table 1.** $(Ca,Sr,Ba)_3Al_2O_6$ as sacrificial layers in literature.

| Material | Sacrificial layer | | | | | | | |
|---|---|---|---|---|---|---|---|---|
| | Synthesis method | Synthesis condition | | Target material | Substrate | Transfer method | Etchant, temperature, time | Comments |
| $Sr_3Al_2O_6$ | PLD | $T$ | 670–900 °C | $SrTiO_3$[12,19–23] | $SrTiO_3$ | PDMS | Water | $(Ca,Sr,Ba)_3Al_2O_6$ |
| | | $P_{O_2}$ | $1.0 \times 10^{-6}$ - | $La_xSr_{1-x}MnO_3$[19,28,58] | (001) | PMMA | RT | Tunable lattice |
| | | | ~0.27 mbar | $BaTiO_3$[59–63] | $SrTiO_3$ | PPC/PMMA | 5 m | parameter |
| | | or | | $BiFeO_3$[64,65] | (110) | PET/PMMA | (~90 nm) | |
| | | $P_{Ar}$ | $\sim 6.7 \times 10^{-6}$ mbar | $SrRuO_3$[27,60] | $SrTiO_3$ | PPC/PDMS | 1 h | |
| | | $E$ | 0.8–2.0 J·cm$^{-2}$ | $LaNiO_3$[66] | (111) | PET/PDMS | (~50 nm) | |
| | | | | $BiMnO_3$[67] | | PET/ PEDOT:PSS | 1 d | |
| | | | | $Sr_2IrO_4$[68] | | PI tape | (~9 nm) | |
| | | | | $Fe_3O_4$[69,70] | | PET | | |
| | | | | $CeO_2$[71] | | epoxy | | |
| | | | | $La_{0.7}Ca_{0.3}MnO_3$[72] | | Photoresist | | |
| | | | | $[(La_{0.7}Sr_{0.3}MnO_3)_5/(SrTiO_3)_5]_n$[12,19,35] | | | | |
| | | | | $BaTiO_3/La_{0.7}Sr_{0.3}MnO_3$[73] | | | | |
| | | | | $BaTiO_3/La_{0.7}Sr_{0.3}MnO_3/BaTiO_3$[13] | | | | |
| | | | | $LaAlO_3/YBa_2Cu_3O_{7-x}/LaAlO_3$[74] | | | | |
| | | | | $La_{0.7}Sr_{0.3}MnO_3/BiFeO_3$[75] | | | | |
| | | | | $BiFeO_3/La_{0.67}Sr_{0.33}MnO_3$[76] | | | | |
| | | | | $BaTiO_3$-$CoFe_2O_4$[77] | | | | |
| | MBE | $T$ | 750–950 °C | $SrTiO_3$[11,78] | $SrTiO_3$ | PI tape | | |
| | | $P_{O_2}$ | $1.29 \times 10^{-11}$ – | $BiFeO_3$[79] | (001) | PEN/epoxy | | |
| | | | $1.33 \times 10^{-6}$ mbar | $PbTiO_3$[25] | | | | |
| $Sr_2CaAl_2O_6$ | PLD | $T$ | 710 °C | $SrTiO_3$[32] | | PPC | Water | |
| | | $P_{Ar}$ | $\sim 5.3 \times 10^{-6}$ mbar | n-$SrTiO_3$/n-$PbTiO_3$/n-$SrTiO_3$[33] | | PMMA | RT | |
| | | $E$ | 1.35 J·cm$^{-2}$ | $[(PbTiO_3)_{16}/(SrTiO_3)_{16}]_8$[33] | | | - | |
| $Sr_{1.5}Ca_{1.5}Al_2O_6$ | PLD | $T$ | 700 °C | $SrRuO_3$[34] | | PDMS | Water | |
| | | $P_{O_2}$ | $2 \times 10^{-3}$ mbar | | | | RT | |
| | | $E$ | 2.0 J·cm$^{-2}$ | | | | 12 h | |
| $SrCa_2Al_2O_6$ | PLD | $T$ | 700 °C | $La_{0.7}Ca_{0.3}MnO_3$[31] | | PPC/PMMA | Water | |
| | | $P_{O_2}$ | $\sim 6.7 \times 10^{-6}$ mbar | | | | RT | |
| | | $E$ | 1.25 J·cm$^{-2}$ | | | | - | |
| $Ba_3Al_2O_6$ | PLD | $T$ | 850 °C | La:$BaSnO_3$[30] | | PPC/PDMS | Water | |
| | | $P_{O_2}$ | $\sim 1.3 \times 10^{-7}$ mbar | | | | RT | |
| | | $E$ | 1.5 J·cm$^{-2}$ | | | | 5–10 m | |
| | | $P_{O_2}$ | ~ 0.08 mbar | | | | | |

The synthesis method of each sacrificial thin film is shown along with synthesis conditions, substrates, and etching conditions; In the table, $T$, $P_{O_2}$, $P_{Ar}$, and $E$ indicate the synthesis temperature, pressure of oxygen gas, pressure of argon gas, and laser energy density, respectively; The list of perovskite oxide membranes obtained, the substrate, and the transfer method are also shown; In the column of etching condition, water and RT represent deionized water and room temperature; d, h, and m denote days, hours, and minutes, respectively.

can largely improve the quality of the released membranes by hindering the formation of cracks,[55] which has motivated the exploration of sacrificial layers such as $Ca_2SrAl_2O_6$ (3.852 Å), $Ca_{1.5}Sr_{1.5}Al_2O_6$ (3.882 Å), $Sr_2CaAl_2O_6$ (3.907 Å), and $Ba_3Al_2O_6$ (4.124 Å).[56,55,52–54] However, small Ca ions can make more distorted geometries leading to less structural compatibility with perovskites and reduced water solubility.[57]

Table 1 presents a list of references where $(Ca,Sr,Ba)_3Al_2O_6$ was used as sacrificial layer for obtaining oxide membranes, along with the synthesis method and the main synthesis conditions used in literature. It is interesting to note that in order to achieve a good crystal quality, SAO sacrificial layers are usually grown at high temperatures (700–900 °C) and low oxygen partial pressure ($10^{-6}$–$10^{-5}$ mbar). Nevertheless, it was observed that, at these temperatures, cationic interdiffusion between the sacrificial and the functional layer can occur, especially along misfit dislocations or vertically extended defects.[44] As a matter of example, cationic intermixing between SAO and $La_{0.7}Sr_{0.3}MnO_3$ thin films at 900 °C may cause a phase transformation of the sacrificial layer, making it water-insoluble.[19] Interestingly, Baek et al. showed that the inclusion of a few-unit-cells of $SrTiO_3$ (STO) between the SAO and $La_{0.7}Sr_{0.3}MnO_3$ entirely blocks Mn and La diffusion into the sacrificial layer and avoids the structural transformation, preserving the water solubility.[19] Moreover, 6 u.c. of STO capping layer was also found to protect the sacrificial layer from air humidity, making this heterostructure a practical template for ex situ epitaxial growth using other techniques.[58]

$(Ca,Sr,Ba)_3Al_2O_6$ can be immersed in deionized water at room temperature to dissolve the sacrificial layer and release

**Table 2.** The experimental information of other oxides as sacrificial layers.

| Sacrificial layer | | | | Target material | Substrate | Transfer method | Etchant, temperature, time | Comments |
|---|---|---|---|---|---|---|---|---|
| Material | Synthesis method | Synthesis condition | | | | | | |
| $La_{0.7}Sr_{0.3}MnO_3$<br>$La_{0.67}Sr_{0.33}MnO_3$ | PLD | $T$<br>$P_{O_2}$<br>$E$ | 650–800 °C<br>~0.03–2.7 mbar<br>1.0–2.0 J·cm$^{-2}$ | $PbZr_{0.2}Ti_{0.8}O_3$[40–44]<br>$[(CaTiO_3)_n/(SrTiO_3)_n]_6$[40]<br>$BiFeO_3/SrRuO_3$[40]<br>$LiFe_5O_8$[46]<br>$SrRuO_3/BaTiO_3/SrRuO_3$[45]<br>$Ba_{1-x}Sr_xRuO_3/Ba_{1-x}Sr_xTiO_3/Ba_{1-x}Sr_xRuO_3$[45]<br>$BaTiO_3$[47] | $SrTiO_3$ (001)<br>$GdScO_3$ (110) | PMMA<br>PS/PMMA<br>PI tape<br>PPC/PDMS | KI + HCl solution<br>-<br>1 d | - |
| $SrRuO_3$ | PLD | $T$<br>$P_{O_2}$<br>$E$ | 600–615 °C<br>0.1–0.12 mbar<br>1.5 J·cm$^{-2}$ | $La_{0.7}Sr_{0.3}MnO_3$[48]<br>$LaAlO_3/SrTiO_3$[49] | $SrTiO_3$ (001) | PDMS | $NaIO_4$ (0.4 M)<br>RT<br>Few h - 2 d | - |
| $SrVO_3$ | PLD | $T$<br>$P_{O_2}$ | 760 °C<br>1.2 × 10$^{-6}$ mbar | $SrTiO_3$[50] | | PDMS<br>PET/silicon film | Water<br>50 °C<br>5 d | Small lattice parameter |
| $YBa_2Cu_3O_7$ | PLD | $T$<br>$P_{O_2}$ | 750 °C<br>~0.08 mbar | $SrRuO_3$[80]<br>$La_{0.7}Sr_{0.3}MnO_3$[80,81] | | PMMA | HCl (0.6%)<br>-<br>Few m | Short etching time |
| $SrCoO_{2.5}$ | PLD | $T$<br>$P_{O_2}$<br>$E$ | 750 °C<br>~0.13 mbar<br>1.1 J·cm$^{-2}$ | $SrRuO_3$[53] | $SrTiO_3$ (001)<br>$SrTiO_3$ (110)<br>$SrTiO_3$ (111) | PDMS | Vinegar, 36% $CH_3COOH$ and carbonated drinks<br>RT<br>-<br>3–10 m | |
| BaO | PLD | $T$<br>$P_{O_2}$<br>$E$ | 400 °C<br>~1.3 × 10$^{-5}$ mbar<br>- | $BaTiO_3/SrTiO_3$[54] | $SrTiO_3$ (001) | PET/PDMS | Water<br>-<br>> 10 h | Epitaxial growth on $SrTiO_3$ (001) |
| MgO | PLD | $T$<br>$P_{O_2}$<br>$E$ | 600 °C<br>~2.7 × 10$^{-2}$ mbar<br>- | $CaFe_2O_4$[55] | $SrTiO_3$ (001) | PS | $(NH_4)_2SO_4$ (10%)<br>80 °C<br>12 h | - |

The synthesis method for each sacrificial material is shown with synthesis conditions, target material, substrate, transfer method, and etching conditions; In the table, $T$, $P_{O_2}$, $P_{Ar}$, and $E$ indicate the synthesis temperature, pressure of oxygen gas, pressure of argon gas, and laser energy density, respectively; In the column of etching condition, water and RT represent deionized water and room temperature; d, h, and m denote days, hours, and minutes, respectively.

the freestanding membranes. The time it takes to remove the $(Ca,Sr,Ba)_3Al_2O_6$ sacrificial layer depends on the composition and the thickness of the sacrificial layer, see Table 1. In the case of $Ca_3Al_2O_6$, the sacrificial layer is weakly soluble in water because of the strong Ca—O bonding.[59] However, the solubility can be tuned by substituting Sr or Ba for Ca, which increases the thermodynamic driving force for the cation hydration.[12,56,54] For example, it takes 5—10 min to fully dissolve the 16 nm thick $Ba_3Al_2O_6$ layer while it takes around 1 day for SAO of similar thickness (Table 1).[56] Regarding the thickness dependence, the sacrificial layer dissolving time is reduced as the thickness of the layer increases. For the SAO, it takes 1 day (5 min) to dissolve a film thickness of 9 nm (90 nm).[12] Last, it is worthwhile to mention that target materials might also react with water, for example, $BaTiO_3$ (BTO), which could lead to Ti ion displacements in the $TiO_2$ plane and surface oxygen vacancies due to the hydroxylation of the first BaO layer.[60,61] Therefore, care should be taken when choosing the sacrificial layers and the target material.

### 2.1.2. Perovskite Oxides and Other Oxides

Perovskite oxides such as $La_xSr_{1-x}MnO_3$ (LSMO),[62–69] SRO,[70,71] $SrVO_3$ (SVO),[72] have also been demonstrated as sacrificial layers, see **Table 2**. Compared with the complex crystal structure of the $(Ca,Sr,Ba)_3Al_2O_6$, these sacrificial layers have in most cases the same structure as the target perovskite films, which could potentially help in preserving the in-plane orientation and retain the structural quality of the transferred film. In the case of LSMO sacrificial layer, the chemical reaction for selective etching of LSMO is based on the reduction of the insoluble $Mn^{4+}$ to soluble $Mn^{2+}$ by $Cl^-$ according to the following reaction[73]

$$MnO_2 + 4H_3O^+ + 2Cl^- \rightarrow Mn^{2+} + 6H_2O + Cl_2 \quad (1)$$

However, if $Mn^{4+}$ is not completely reduced, insoluble $MnO_2$ precipitates are left behind. As a matter of example, Elangovan et al. have grown BTO/LSMO heterostructure on STO

(001) to realize BTO freestanding membranes.[69] The single-crystalline BTO film was released by selective etching of the LSMO in an aqueous solution of KI + HCl + $H_2O$. Negligible chemical etching of BTO was observed due to the much faster etch rate of LSMO with respect to BTO.

Dissolving of SRO is realized by oxidizing $RuO_2$ into volatile $RuO_4$ within aqueous solution:

$$SrRuO_3\,(s) + 2H_3O^+ + 2IO_4^- \rightarrow Sr^{2+}\,(aq) + RuO_4\,(aq) + 3H_2O + 2IO_3^- \quad (2)$$

Weber et al. have investigated the etching rate of SRO with different etchants and selected $NaIO_4$ solution with a suitable etching rate (2 nm $s^{-1}$) and near-neutral pH.[79] Using this approach, Pesquera et al. grew LSMO epitaxially on STO mediated by an SRO sacrificial layer, which was subsequently dissolved by selective etching without damaging the LSMO film.[70] This approach is also used to fabricate single-crystalline freestanding membranes of LAO/STO heterostructures and directly integrated the membrane on sapphire substrate via vdW stacking.[71]

$SrVO_3$ is another sacrificial layer candidate, which is suitable for the growth of a wide spectrum of perovskites due to its cubic structure ($a$ = 3.84 Å). Compared with LSMO or SRO that requires complex etchants, SVO can be dissolved in water.[72] This material would expand the choice of water-soluble materials especially for those materials that are not chemically stable against stronger acids. However, special caution is needed because SVO is toxic.

Recently, $SrCoO_{2.5}$ (SCO) has been also proposed as generic sacrificial layer for a facile epitaxy of perovskite oxides thin films.[76] SCO presents a brownmillerite structure with an in-plane lattice parameter close to the STO ($a$ = 3.90 Å) and can be epitaxially grown on many perovskite substrates with different crystallographic orientations. Moreover, SCO can be dissolved in weak acetic acid solutions, in vinegar and in common carbonated drinks, which allows a safe transfer process of perovskite membranes.

Beside perovskite oxides, metal oxides were also proposed as sacrificial layers, such as BaO,[77] MgO,[78] ZnO,[80] and $VO_2$.[81] BaO has a rock salt structure with a lattice parameter of 5.539 Å. The lattice mismatch with STO is small (0.31%) as a result of the 45° rotation when coherently grown on the STO (001) substrate, see Figure 2b.[77] Takahashi and Lippmaa have fabricated BTO/STO freestanding membranes using BaO as a sacrificial layer.[77] This BaO sacrificial layer was dissolved by water after 10 h as a result of the reaction between BaO and water: BaO + $H_2O \rightarrow Ba(OH)_2$. Various combination of the sacrificial layer and etchant have been developed, for example, MgO, ZnO, and $VO_2$, and were used to fabricate non-perovskite oxides, such as $CaFe_2O_4$, $VO_2$, and $TiO_2$.[77,78,80,81] However, such sacrificial layers are not suitable to fabricate freestanding membranes with a perovskite structure due to the large lattice mismatch.

### 2.1.3. Transfer Methods for Freestanding Oxide Thin Films

The transfer and manipulation of single-crystals membranes is an essential part of wet etching methods, since the integrity and quality of the membrane is largely affected by the releasing process and handling techniques.[31,42,82] Common methods used for perovskite oxides membranes mimics the well-developed wet transfer process of 2D vdW materials, such as graphene[83,84] and TMDC,[85,86] and generally involve three major steps: lifting off the film, stamping the free-standing film onto the desired substrate and last, removing the stamp layer (also called support layer). **Figure 3** shows the main strategies adopted in literature for transfer and manipulation of perovskite oxide membranes.

The first step is the etching process where the oxide film is detached from the growth substrate by selectively etching the sacrificial layer, as described above (see Table 1 for the list of etchants and optimized condition for each sacrificial layer). To prevent crinkling and folding of the free-standing membranes during the etching release process,[82] a common way is to cover a support layer on the oxide membrane to facilitate the lifting off and follow-up transferring, just as polymer-supported is used for transfer of graphene.[84] Many polymer materials have been developed and used as support layers, considering the merits of flexibility, mechanical strength, and adhesive contact, such as polyimide (PI) tape, polydimethylsiloxane (PDMS),[11,12,82,87] polymethyl-methacrylate (PMMA),[20,62] polystyrene (PS), or the combination of these materials, like polypropylene carbonate (PPC)-PDMS stack[13,62,87] and PI sheet with PPC layer.[52,67]

PMMA, which is most commonly used in transferring of chemical-vapor-deposited graphene,[38,84] has also found a wide application in the transfer of oxide membrane.[20,62,42] PMMA can be easily coated on the oxide surface, and washed away by acetone once the transfer is completed, see Figure 3a. However, the polymer residues and the contamination associated with this process are always hard to be removed.[88] Moreover, it was found that the PMMA on the oxide stack may not be fully in contact with the transfer substrate, which can result in unattached regions that tend to form bubbles and ripples or in the cracking of the membrane during the dissolving process of PMMA.[42,83] Zhang et al. has introduced a frame structure consisting of polyethylene terephthalate (PET) and PMMA to stamp the SRO film, achieving a high yield transfer rate without macroscopic cracking.[42]

Thermal release polymer sheets such as PDMS have been also explored as candidates for support layers, see Figure 3b. Instead of chemically etching in the final step, the polymer can be handily released by heating up to 70 °C, which facilitates the removal of residues and the membrane cleanliness.[12] However, cracks and tears can be introduced inevitably when peeling off PDMS from the membrane, making it difficult to obtain continuous membranes.[82] A two-layer structure was also designed to improve this method, for example, PPC-PDMS stack.[13,62,87]

Scotch tape, like PI tape, has been used to transfer large area oxide membranes through adhesion, see Figure 3c.[28,68] However, the downside of this method is that it is impossible to remove the adhesive tape from the membrane at the final step. Steady transfer operation should be guaranteed, otherwise the freestanding membrane may easily bend and crack.

A support-free transfer method was also proposed by Gu et al.,[31] see Figure 3d. In their work, they showed that crack-free membranes of SRO and BTO could be obtained by scooping the freestanding membranes floating on the surface of the solvent after the dissolution of the sacrificial layer. Interestingly, in their

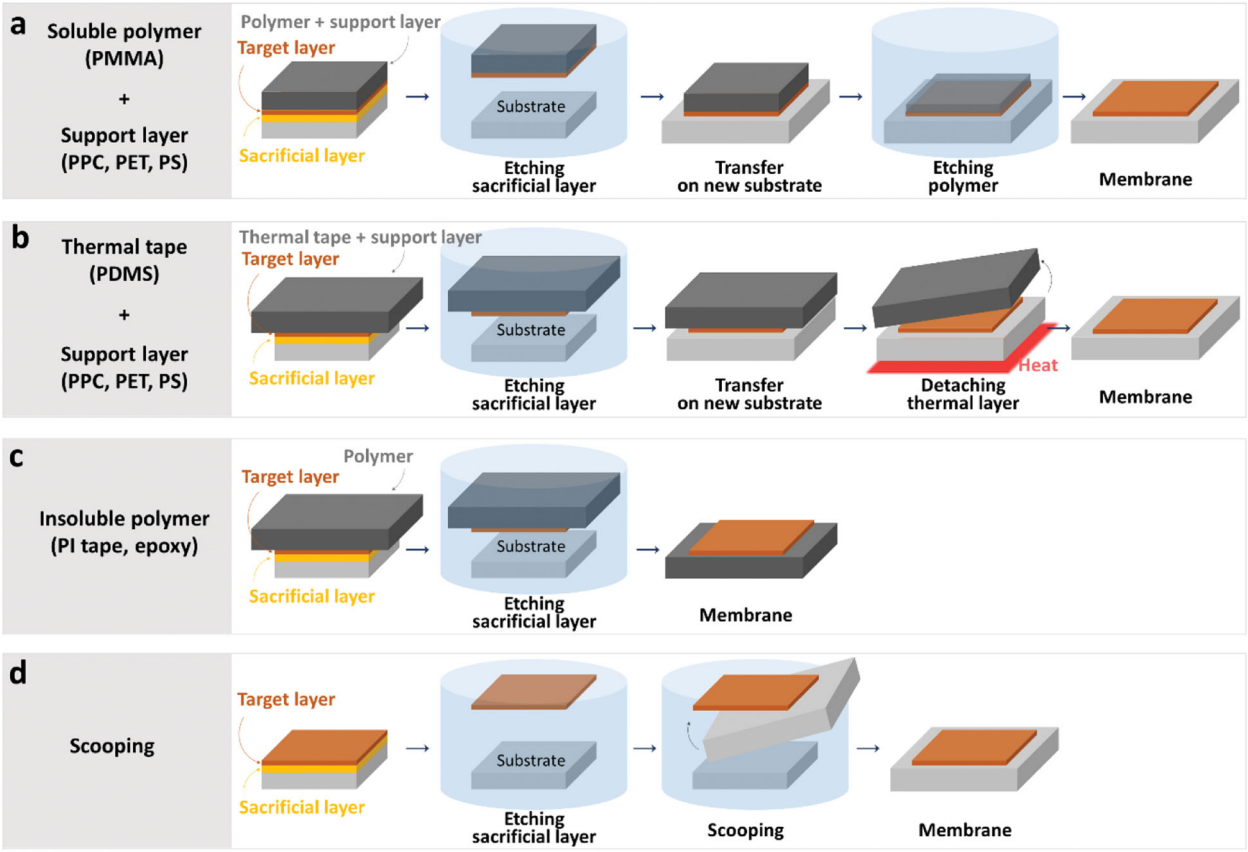


**Figure 3.** Sketch of the main transfer strategies used for the release and transfer of perovskite oxide membranes via wet etching method: a) Soluble polymer, b) Thermal tape, c) Insoluble polymer and d) Scooping of the floating membrane.

work they also showed that the substrate, after the membrane releasing, could be reused for other depositions.

The enormous progress in the development of 2D materials transfer such as graphene and TMDs over the last decades, can be a good starting point for successfully and fast progress of transfer methods for perovskite oxide membranes. The polymer-assisted transfer method has been demonstrated to yield a single-crystal oxide membrane with macroscopic dimensions (hundreds of micrometers to millimeters). However, considering the hardness and brittleness of oxide membranes, as well as the issues such as cracks, wrinkles, trapped bubbles, and polymer residues, the question of how to develop techniques for transferring single-crystal oxide membranes with sufficient size, as-grown uniformity, and high-quality onto arbitrary substrate remains a key challenge.

### 2.2. Mechanical Exfoliation

In the last few years, the quest for flexible oxide electronics has motivated the development of mechanical exfoliation methods for integrating oxide thin films into complex devices.[89] Mechanical exfoliation is a technique based on the deposition of target thin film onto a 2D layered material, followed by the cleavage of the deposited layer along the heterointerface (Figure 1b).[90] 2D layered materials are structures characterized by weak bonds between the constitutive layers. This allows thinning the 2D-layered substrate along these planes, reducing progressively its thickness and increasing its flexibility, eventually achieving membranes. Moreover, the integration of well-ordered epitaxial structure into 2D layered substrates can be achieved even for dissimilar crystalline structure, through quasi-van der Waals (qvdW) epitaxy.[91–93] In traditional epitaxy, strong chemical bonds between the thin film and the substrate determine the orientation and structural characteristics of the layers, intrinsically limiting the choice of substrates materials. Indeed, when the lattice constants of the substrates strongly differ from the thin films, structural dislocations or random orientation of grains tend to appear in the layers, in order to minimize the elastic strain energy of the system. On the contrary, vdW epitaxy consists in the creation of weak bonds between the film and the substrate, which allows the growth of relaxed and epitaxial thin layers with unrelated orientation with the substrate.[94–96] The deposition of 3D structures on 2D layered materials can take place through the qvdW epitaxy, a mixed behavior based on the initial creation of an interface with vdW bonds followed by traditional homoepitaxial growth of the layer.[97] The weak interaction between the oxide layers and the substrates offers the opportunity of creating freestanding membranes by exfoliating the top layers.[98]

A characteristic example of 2D-layered material used for the integration of perovskite oxide is mica, a large family of phyllosilicate minerals possessing a monoclinic structure

layered along the 001 plane. Mica possesses general formula $X_2Y_nZ_8O_{20}(OH,F)_4$, where X, Y and Z are the interlayer cation (e.g., K and Na), the octedrahedrally coordinated atom (e.g., Al and Mg) and the tetrahedral coordinated element (Si, Al, etc.), respectively. The most commonly used micas for the thin film integration are the muscovite ($n = 4$, e.g., $KAl_2(Si_3Al)O_{10}(OH)_2$) and the pholgopite ($n = 6$, e.g., $KMg_3(Si_3Al)O_{10}F_2$).[93] Mica is emerging as one of the most interesting substrates for flexible electronic, due to its superior mechanical properties and its good compatibility with oxides´ deposition processes.[92,93] The epitaxial growth of perovskite oxides on Mica has been generally interpreted in the light of qvdW epitaxy.[91–93,99] Nevertheless, Lu et al.[100] recently showed that strong bonds can be formed at the interface between pholgopite mica and STO thin films deposited by PLD, resulting in the epitaxial relation $\{111\}_{STO}||(001)_{mica}$ (in-plane $\langle 110\rangle_{STO}||[100]_{mica}$ and $\langle 112\rangle_{STO}||[010]_{mica}$), see **Figure 4**. Despite the different cationic rearrangements of these orientations, the epitaxial match is allowed by an almost identical rearrangement of the oxygen sublattices of the two compounds.[100] A similar (111) orientation was also observed for other perovskites thin films deposited on mica (001), such as SRO/BTO,[101] $SrVO_3$,[102] Eu-doped $0.94Bi_{0.5}Na_{0.5}TiO_3$–$0.06BaTiO_3$,[99] $CaVO_3$/STO,[103] and $La_{0.7}Sr_{0.3}MnO_3$/STO.[104] Nevertheless, other types of orientations and even polycrystalline thin films are reported in literature for perovskite oxides deposited on mica substrates.[105–107] In this sense, Ko et al. found that the $PbZrO_3$/SRO heterostructure tends to develop multiple orientations if directly grown on muscovite mica, while well-oriented (111) thin films can be obtained by the insertion of a 1-nm-thick $CoFe_2O_4$ seeding layer.[108] These results show that different types of crystallographic orientations and bonding can be expected at the perovskite/mica interface. The possibility of cleaving $La_{0.7}Sr_{0.3}MnO_3$ thin films from mica substrates was demonstrated by Zhang et al.[98] In their work, the authors showed that polycrystalline LSMO thin films could be easily peeled off by muscovite mica due to the weak interaction between the film and the substrate. Additionally, mica can be cleaved along the weak bonded constitutive planes after the thin film deposition, increasing the flexibility of the structure and allowing the study of bending strain effect on the perovskite layers (see Section 4.2).[93,101]

Another promising 2D material that can be used for the mechanical exfoliation of perovskite oxide thin films is graphene. Lee et al. showed that STO thin films with predominant (001) orientation can be directly grown on graphene covered $SiO_2$/Si substrates by PLD.[109] The thermal oxidation of graphene can be avoided during the film growth by using low oxygen partial pressure ($\approx 10^{-6}$ mbar). The interface between the STO and the graphene is characterized by moderate bonding, as suggested by the presence of moderate lattice strain in the oxide layer.[109] Interestingly, Kum et al. showed that graphene can be used as a universal mechanical exfoliation method for obtaining freestanding oxides thin films.[14] In their work, the authors showed that epitaxial STO (001) thin films can be grown on double-layer graphene-coated STO (001) single-crystals through remote epitaxy, a mechanism based on the semitransparency of the graphene layer to the atomic potential fields of the STO substrate. Moreover, the thin films can be transferred to other substrates thanks to the weak bonds between graphene and the perovskite layer. These results show that graphene-based remote epitaxy has emerged as a promising method for obtain large area freestanding thin films.

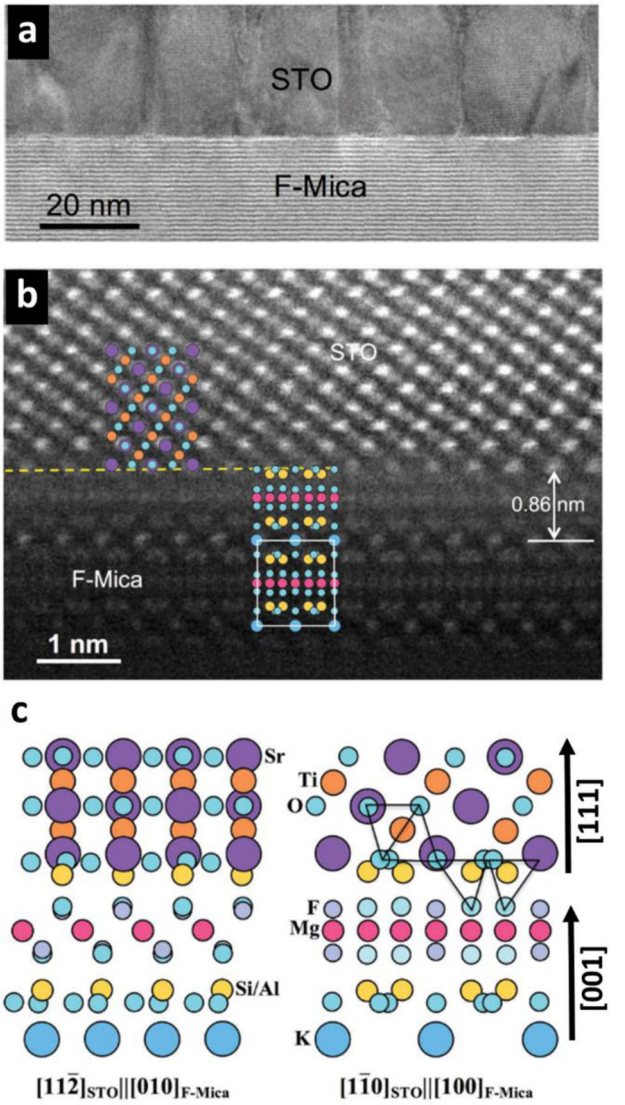


**Figure 4.** Epitaxial growth of $SrTiO_3$ on Mica. a) Low magnification TEM and b) STEM high angle angular dark field image of an STO thin film grown on Mica. c) Reconstruction of the epitaxial relation and reconstruction of the interface between the (001) mica and the (111) STO thin films. The epitaxial relation is ensured by a similar arrangement of the oxygen sublattice. Reproduced under terms of the CC-BY 4.0 license.[100] Copyright 2020, Wiley-VCH.

### 2.3. Self-Formed Freestanding Films through Spalling

As an alternative to the method based on sacrificial layers and epitaxial liftoff[110] freestanding membranes of brittle crystals can be produced by inducing and controlling the fracture mode known as spalling. The basic mechanisms and elements of the technique are illustrated in Figure 1c: A tensile strained top layer is deposited on the crystal/wafer of interest and under sufficient stress and sufficient bonding strength, the crystal will form

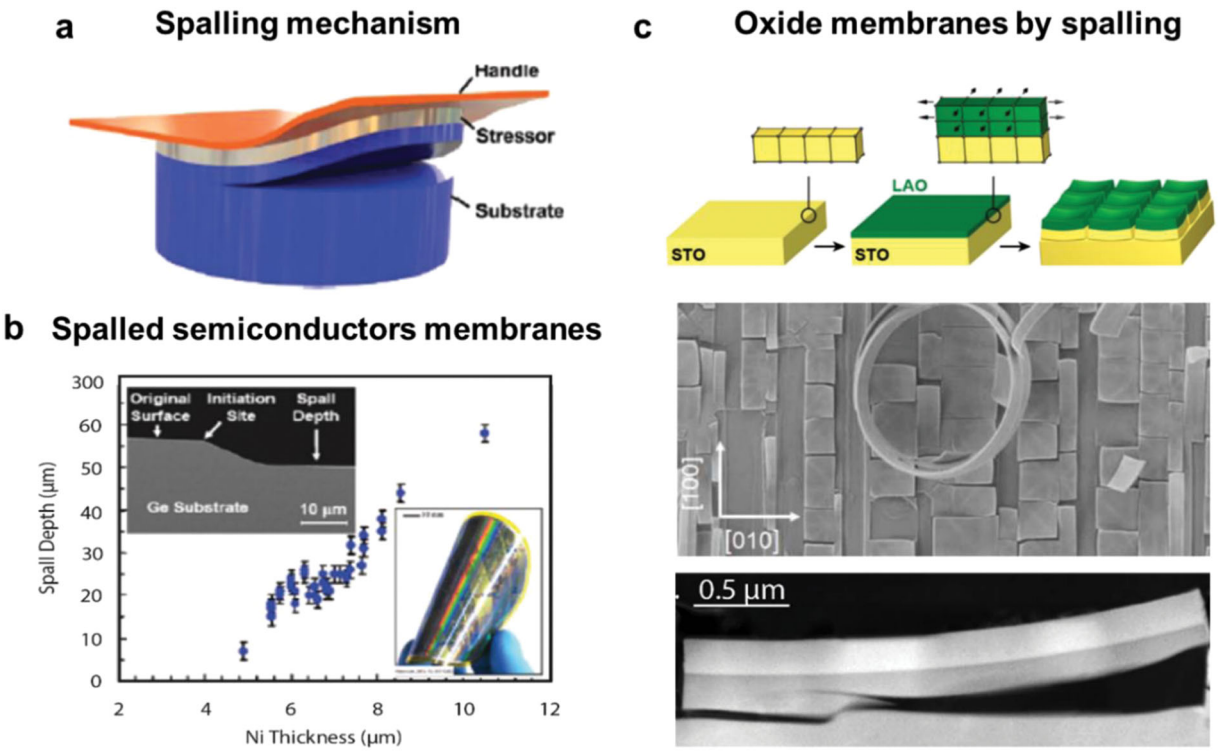


**Figure 5.** Self-formed membranes through spalling. a) Illustration of the spalling mechanism. b) Evolution of the spalling depth of the fracture plane as a function of the thickness of the stressor for Ge single-crystals. c) Schematic representation and SEM images of spalling mechanism of LAO thin films deposited on STO (001). a,b) Reproduced under terms of the CC-BY license from Bedell et al., 2013, IOP Science. The inset of (b) is adapted with permission.[115] Copyright 2013, American Chemical Society. c) Top panel reproduced with permission.[16] Copyright 2021, American Chemical Society. Bottom two panels reproduced with permission.[15] Copyright 2020, Wiley-VCH.

cracks which propagate through the crystal. Different types of substrate fractures may occur, the most familiar being the vertical cracking through the entire crystal leading to breaking of the wafers. However, under certain conditions of tensile strained top-layers on brittle crystals, the interplay of the shear- and opening-stress at the tip of a crack may direct the propagation parallel to the surface at a stable depth. This fracture mode is known as spalling and relies on a stable propagation of the fracture mode parallel to the substrate at the equilibrium depth where the shear stress is minimized. The process is self-correcting: for a crack too close to the surface, the crystal above the crack will contract upon fracturing and the crack propagation is deflected downward. Conversely, for a crack very deep in the substrate the top layer will expand upon fracture due to the curvature of the membrane and the crack is instead deflected upwards.[111] The resulting steady-state crack propagation is thus parallel to the surface at a depth that depends on the mechanical properties of the crystals. The phenomenon and its mechanism was first analyzed in detail by Hutchinson et al.[111] It is important to note that the mechanism is purely mechanical, that is, it does not require defects, inhomogeneities, or anisotropies and applies in general for material combinations with the required mechanical properties.

Substrate spalling has been investigated for the realization of semiconductor membranes. Dross et al.[112] obtained silicon membranes of areas up to 25 $cm^2$ and thicknesses of 30–50 microns by deposition/bonding of Ag and Al films on silicon and inducing the strain by the difference in the coefficients of thermal expansion upon cooling the sample after annealing. The metal film was then selectively etched and the high-quality spalled silicon films were used to fabricate functional solar cells. The method has been generalized and optimized, including the introduction of flexible handle layers to support and control the initiation of the fracturing rather than the spontaneous spalling of early works. Wafer scale spalled membranes of germanium, nitrides, and III–V compounds have been successfully produced[113,114] and also the release of free-standing semiconductor membranes containing functional elements and electronic devices and circuits have been in demonstrated as a viable route toward flexible electronics.[115,116] The thickness of the spalled membranes depends on the mechanical properties, stresses, and thicknesses[113] of both the target crystal, the stressor material and possible handle-layers. For example, for the same materials, there is an approximately linear relationship between the thickness of the stressor and the depth of the fracture plane (see **Figure 5**b). This enables good control of the spalling process and thicknesses from hundreds of angstroms to hundreds of micrometers have been achieved.[117] No fundamental barrier seems to hinder spalling of films of only a few nanometers.

Until now, the spalling method has been developed in the context of semiconductors, however, recently, the viability of the method was demonstrated also for oxides.[15] Epitaxial LAO/STO heterostructures with 70–100 nm LAO top layers were grown by PLD, and the LAO/STO lattice mismatch LAO experiences

tensile epitaxial needed for activating the spalling process. No handle layers were used to direct the fracturing and provide mechanical support of the membrane, which resulted in a combination of vertical and spalling fracturing, leaving a mosaic of micrometer scaled membranes on the sample surface (Figure 5c). As expected for the spalling process, the parallel fracture occurred below the tensile LAO and each membrane contains an LAO/STO interface. Dahm et al.[16] showed that by pre-patterning of the growth substrate using lithography and ion milling, the lateral locations of cracks can be controlled. This procedure enabled the controlled formation of free-standing LAO/STO micro membranes with sizes from 2 to 20 μm. Also, by mechanical micro-manipulation individual membranes were transferred to silicon substrates and electrical devices were fabricated using lithography.[16]

## 3. Emerging Functionalities in Freestanding Perovskite Thin Films

Perovskite oxide thin films present several functional properties that have allowed their usage in sensors, actuators, surface acoustic wave devices, and memory devices to name a few.[5–7] The continued advancement of oxides in potential applications is however often hampered by the lack of epitaxial integration with important technological platforms such as silicon and flexible materials like PET. Freestanding oxide membranes, on the other hand, provide the possibility to combine oxide perovskite with other materials by means of mechanical transfer (stamping). This possibility has led to significant advances in the field, for example, with demonstration of freestanding $LaAlO_3$/STO membranes on silicon substrates that contain a 2D electron gas exhibiting also superconductivity at low temperature.[15,16] Another important prospect of freestanding membranes is the emergence of different functionalities when compared with the substrate-clamped counterpart. This section will cover representative seminal works where new functional properties not found in the substrate-supported thin film have arisen.

### 3.1. Surface-Induced Changes in the Electronic and Structural Properties

Transitioning from an as-grown to a freestanding state will naturally force the membranes to undergo structural changes, for example, due to the large surface to volume ratio. Ji et al.[11] synthesized high-quality freestanding $BiFeO_3$ films with MBE using the method of Lu et al.[12] They discovered that ultrathin freestanding BFO films show a structural transition from rhombohedral-like phase to tetragonal-like phase when the clamping effect of the substrate is removed, see **Figure 6**a. This effect is especially observed in 3 u.c. thick BFO membranes, where the significant increase of the lattice parameter yielded to a c/a ratio of 1.22 and a polarization of 140 $\mu$C cm$^{-2}$ in the out-of-plane direction.[11] This stands in sharp contrast to the bulk rhombohedral $BiFeO_3$,[118] which only reaches a polarization of 100 $\mu$C cm$^{-2}$ and c/a ratio of 1. Through first principle calculation, they proposed that the large c/a ratio originates from the displacement of Fe from the centrosymmetric position in the tetragonal phase of ultrathin BFO membranes not clamped by the substrate.[11]

Enhanced tetragonality was also observed in ultrathin freestanding STO thin films by Chiu et al.[119] In their work, the authors showed that STO thin films below 10 nm undergo through a transformation from cubic to tetragonal structure when released from the substrate. This phase is characterized by a displacement of Ti atoms from the $TiO_6$ octahedron center and by the appearance of delocalized electrons. A modification of the electronic and magnetic properties was also observed in other perovskites membranes when released from the substrate. Lu et al. showed that ultrathin freestanding $LaMnO_3$ thin films display an exotic soft ferromagnetism along both in-plane and out-of plane direction for thicknesses below 4 nm.[120] This phenomenon, not present in the substrate-supported thin films, is originated by a symmetrical reduction of Mn oxidation state near the membrane´s surface, induced by a protonation of the material during the wet releasing process, which reduces the magnetic anisotropy and leads to the appearance of multidirectional soft ferromagnetism. These works show that surface effects in ultrathin perovskite oxide membranes may give rise to functional properties absent in the substrate-supported thin films.

### 3.2. Enhanced Elasticity and Flexibility

Perovskite oxides in bulk form are usually very brittle and only withstand small tensile strains before fracture.[121] Because of this, conventional oxide thin films grown epitaxially on bulk crystal substrates are tough and very difficult to manipulate mechanically without causing crystal fracturing. However, when the oxide film is released from its epitaxial host by one of the strategies described in this review, it becomes far more flexible.[22,30] Indeed, it was shown that single-crystal perovskite membranes can sustain extremely large tensile strain before breaking.[22,69,30,35,38,122] In particular, Harbola et al. showed that in single-crystal membranes of STO the tensile strain strength can be as high as 6%, almost an order of magnitude more than in bulk form.[22] A non-monotonic change of the Young modulus in nanometric membranes of STO was also observed, due to a competitive behavior of surface elasticity and strain gradient elasticity.[23] Moreover, ferroelectric freestanding perovskite thin films display superelasticity and ultraflexibility at the nanoscale, due to a continuous rotation of the polarization direction and to local phase transformations that avoid mechanical failure.[69,30,35,38,122] More details about this phenomenon and about the effects of strain in freestanding perovskite oxides will be discussed in Section 4 of this work.

### 3.3. Suppression of Mechanical Interaction with the Substrate

Freestanding oxide thin films are characterized by a suppression of the mechanical interaction with the substrate (i.e., absence of the clamping effect). This effect may be particularly relevant in ferroelectric materials, where the clamping effect controls the movement of ferroelastic domain walls and limits the piezoelectric response.[123] Bakaul et al. studied the evolution of ferroelectric domain walls in PZT freestanding thin films.[64] A decrease from two to three orders of magnitude of domain wall velocity was found after the substrate removal. However, this variation does not origin directly from the alteration of the epitaxial

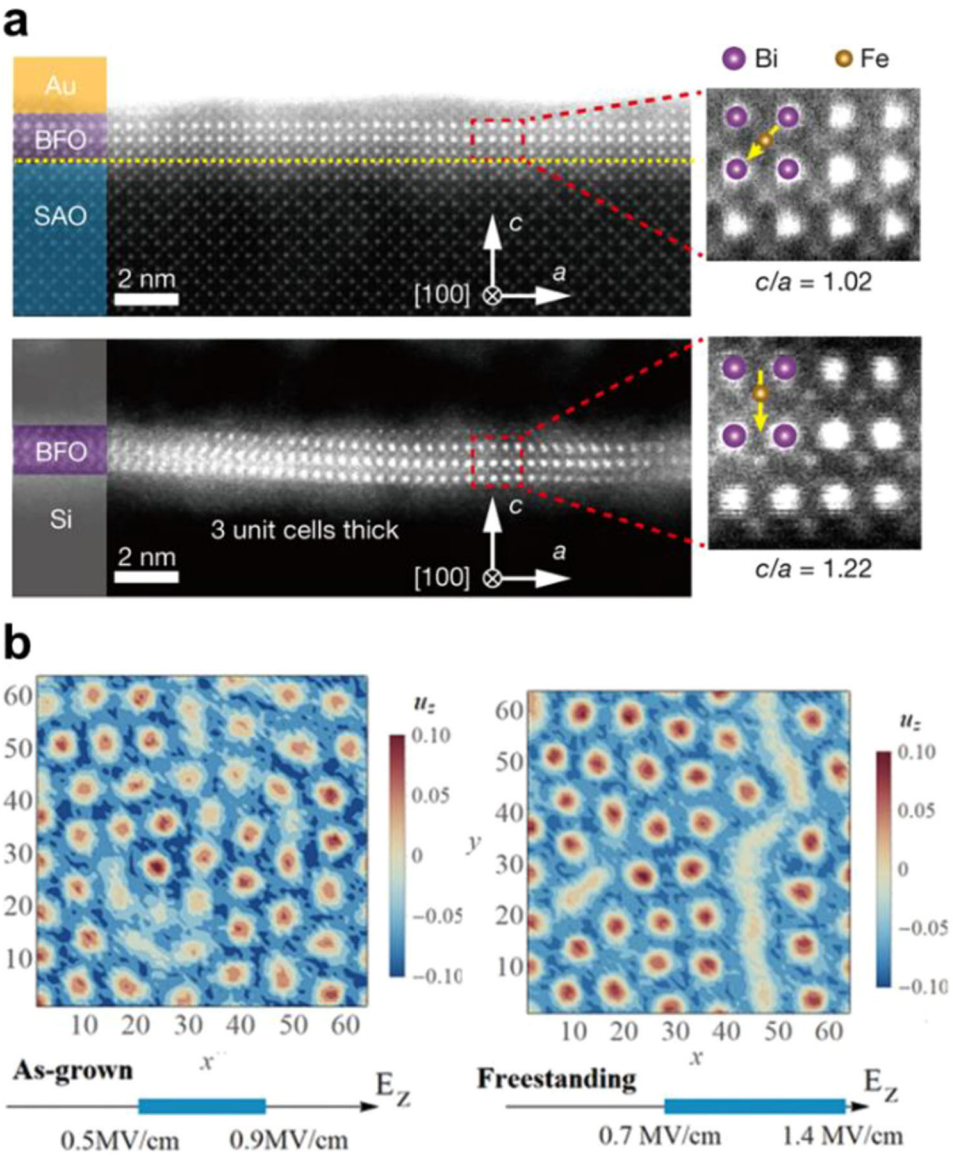


**Figure 6.** a) Giant out of plane polarization in freestanding $BiFeO_3$ thin films below 3 u.c. TEM images shows a large tetragonality and a large out of plane displacement of the Fe atoms after the releasing process. Reproduced with permission.[11] Copyright 2019, Springer Nature. b) Ferroelectric bubble domain in PZT/STO/PZT freestanding membranes. The panel shows the comparison between the out-of-plane polarization component for as grown and freestanding thin films. Reproduced with permission.[65] Copyright 2020, Wiley-VCH.

landscape, but rather from the formation of mesoscopic ripples, generated to release the compressive strain during the membrane fabrication. On the contrary, Pesquera et al. showed that high-quality freestanding BTO membranes sandwiched between SRO thin films electrodes present lower coercive fields and faster domain dynamics compared to substrate-clamped epitaxial BTO.[67] The origin of this change of behavior lies in a reduction of the elastic energy needed for the creation of 90° domain boundaries in membranes upon the substrate removal, favoring the polarization switching of the ferroelectric freestanding thin films.[67]

The possibility of completely detaching the film from the substrate can also give rise to the formation of exotic ferroelectric topologies. Saidur et al. showed that ferroelectric bubble domains can be stabilized in freestanding PZT/STO/PZT heterostructure membranes.[65] These type of ferroelectric topological objects are typically seen as a precursor to electrical skyrmions, which have been shown to arise in ferroelectric–dielectric–ferroelectric heterostructures epitaxially clamped to flat oxide surfaces.[124,125] Comparing the as-grown to the freestanding PZT/STO/PZT system, first principle-based effective Hamiltonian simulations shows that the stress in the free freestanding membranes increases the energy range and the domain size that stabilize the formation of skyrmion bubbles, due to a reduction of the homogenous strain, see Figure 6b.[65] Additionally, Li et al. observed a radical transformation of the polarization direction in $PbTiO_3$/STO superlattice with a SRO bottom electrode when released from its substrate.[126] Interestingly, the variation of the

polarization direction in the superlattice drove the membrane to curl up into microtubes, in order to minimize the overall elastic energy. These results show that the suppression of the mechanical interaction with the substrates may influence the polarization dynamics of ferroelectric perovskite oxides.

### 3.4. 2D Free-Standing Perovskite Oxides

Finally, it is worth mentioning the last advances in the synthesis of perovskite oxides approaching the 2D limit. Hong et al. found that ultrathin membranes of STO below 5 u.c. undergo through a crystalline to amorphous transition when released from the substrate.[20] The collapse of the crystalline order was interpreted in the frame of the Berezinskii–Kosterlitz–Thouless transition, which predicts the proliferation of dislocations below a critical thickness, hindering the long-range crystallinity.[20] Nevertheless, Ji et al. recently showed the possibility of synthetizing single-crystal STO and $BiFeO_3$ down to 1 unit cell, with a good long range crystallinity observed by TEM.[11] These results pave the way to the study of interfacial and 2D phenomena in perovskite oxides thin films.[127]

## 4. Strain Control in Freestanding Perovskite Oxide Thin Films

The profound interplay between structural and electronic properties is one of the most interesting strategy for discovering and control functionalities in perovskite oxides.[128–131] Epitaxial perovskite thin films and heterostructures are largely influenced by strain, especially when the thicknesses of the films are only a few unit cells.[132,133] Indeed, perovskites are well known for their strong coupling between structural distortions and physical properties due to the centrally coordinated octahedra bond flexibility, which allows for a multitude of distortions from the ideal highly symmetric structure.[5] The traditional method for investigating strain effects is based on the epitaxial growth on lattice-mismatched substrates, which results in the generation of misfit strain in the layers. This method, however, limits the maximum achievable strain before structural relaxation of the layers takes place and hinders a deterministic study of the strain effect on the functional properties.[134] Moreover, epitaxial growth of thin films usually requires high temperature conditions, favoring the formation of chemical defects (e.g., oxygen vacancies) and cationic interdiffusion with the substrate.[135] For example, tensile strain reduces the formation energy of oxygen vacancies during growth, which largely modifies the electronic structure and hinders an isolated study of structural effects on the functional properties.[136–138] Additionally, the presence of the oxide substrate, order of magnitudes thicker than the thin film, may impede the measurements of some functionalities, such as the probe of in-plane ionic conductivity in oxygen ionic conductors.[139] For overcoming these limitations, new strategies must be pursued.

Freestanding thin films are emerging as a new platform for investigating extremely large and tunable strain states in perovskite oxides. The most common strategies for controlling lattice strain in thin membranes are 1) multilayer epitaxy of freestanding thin films, 2) mechanical bending, and 3) mechanical stretching (see **Figure 7**). In the following, we review these methods, highlighting the main advantages and drawbacks.

### 4.1. Multilayer Epitaxy in Freestanding Films

Epitaxial strain in multilayer membranes was recently proposed by Pesquera et al. as an alternative method for controlling the strain state of oxide thin films by tuning the lattice mismatch of the multilayers' components.[67] In a single material membrane, the misfit strain imposed by the substrate vanishes in the release process and the layer tends to adopt the bulk equilibrium lattice parameter. In a multilayer epitaxial membrane, the releasing procedure will remove the substrate constraint but the lattice misfit among the layers will determine a residual strain state in the films. Considering the simple case of an oxide thin film epitaxially sandwiched between two symmetrical layers, the lattice mismatch between the components will drive a force with opposite directions on the internal (P) and the eternal layers (−P/2), see Figure 7a. Considering a planar stress condition and no bending of the trilayer membrane, the equilibrium in-plane strain of the internal layer can be calculated as[140]

$$\varepsilon_i = \frac{u_M}{1 + \frac{t_i}{2t_e} \cdot \frac{M_i}{M_e}} \tag{3}$$

where $t_i$ and $M_i$ are the thickness and biaxial modulus of the internal layer, $t_e$ and $M_e$ the thickness and biaxial modulus of the external ones, and $u_m$ the misfit strain between the in-plane lattice parameters of the internal and external thin films ($u_M = \frac{a_i - a_e}{a_i}$). Figure 7b shows the equilibrium in-plane strain of a trilayer membrane calculated as a function of the layers thickness ratio for different bulk misfit strains. The results show that the in-plane strain can be progressively tuned by varying the thickness of the external layers, with a trend that depends on the mechanical properties of the layers. Using this approach, Pesquera et al. achieved the control of the tetragonality of compressive strained ferroelectric BTO sandwiched between $Ba_{1-x}Sr_xRuO_3$ electrodes.[67] Their results show that a deterministic control of the Curie temperature, remanent polarization, and coercive field can be obtained in BTO through compressive strain.

Overall, the main advantage of this method is the possibility of continuously controlling the strain state of oxides by varying the thickness or the composition of the layers. Moreover, a facile measurement of out of plane electrical properties can be achieved by depositing metallic oxides as external layers. Nevertheless, the driving force for the generation of in-plane strain remains the lattice mismatch between the layers, which bears the typical disadvantages of traditional substrate-induced misfit strain and limits its application to oxides that can be coherently grown on each other.

### 4.2. Mechanical Bending

Mechanical bending is the most common way employed in literature to actively control the strain in oxide thin film.[141] Two main types of strategies were developed: 1) bending of layers supported

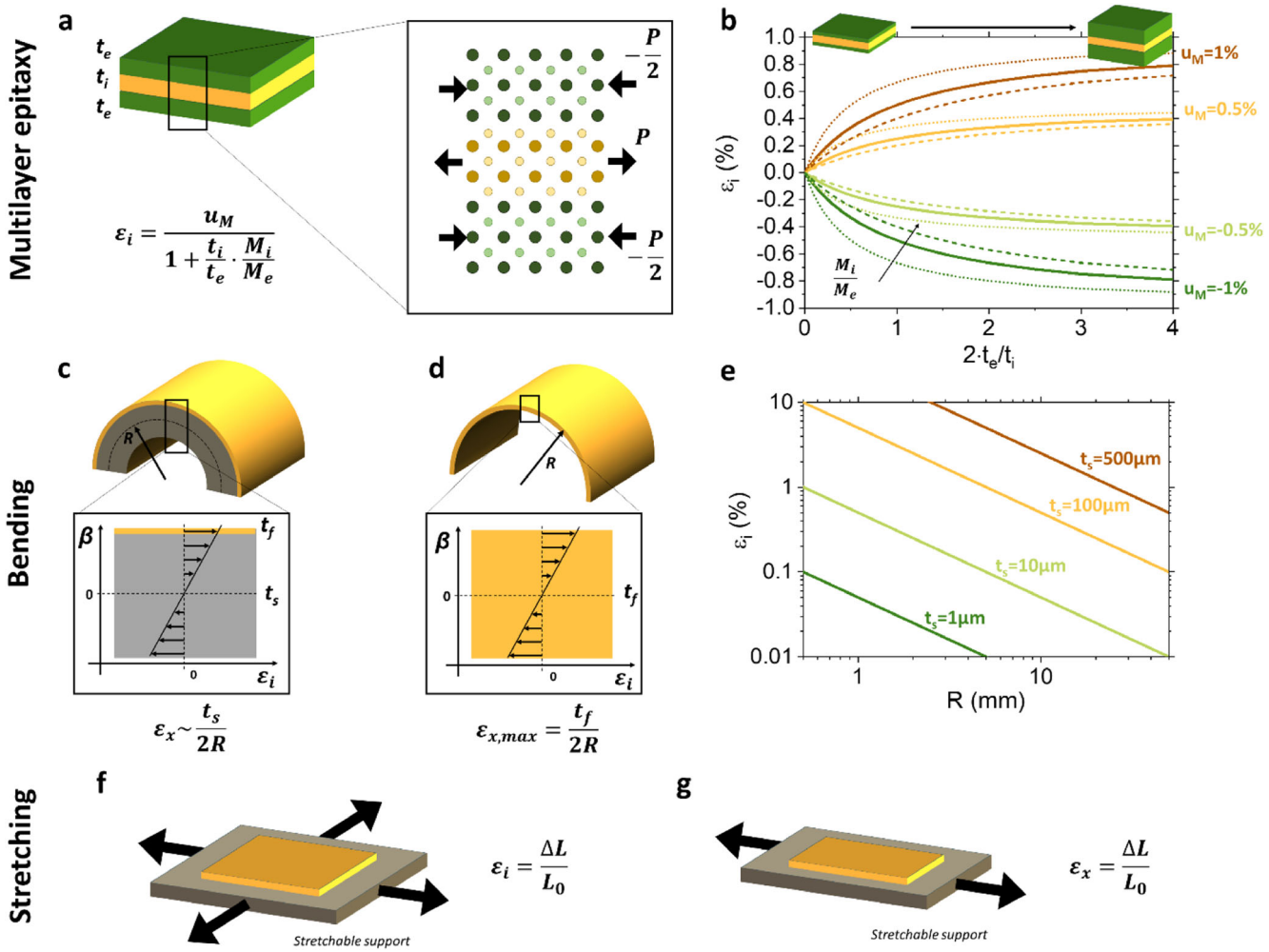


**Figure 7.** Schematic representation of the main strategies for strain tuning in oxide membranes. a) Sketch of a trilayer epitaxial membrane displaying strain due to lattice mismatch between the layers. b) Evolution of the strain in a symmetrical trilayer as a function of the layers thicknesses, for different misfit strains ($u_M$) and elastic Moduli ratios ($M_i/M_e$). Schematic representation of the distribution of strain states in a c) supported and d) self-standing membrane subjected to mechanical bending. e) Maximum bending strain calculated for a supported membrane under different radius of curvature ($R$) and for different substrates thicknesses ($t_s$). Sketch of the f) biaxial and g) uniaxial strain achievable in a membrane under mechanical stretching.

on a flexible or curved substrate (Figure 7c) and 2) bending of self-standing thin films (Figure 7d). In both cases, bending generates an in-plane strain, $\varepsilon_x$, along the bending direction proportional to the distance, $b_i$, from the neutral plane:

$$\varepsilon_x = \frac{\beta}{R} \tag{4}$$

where $R$ is the radius of curvature of neutral plane. Tensile strain develops for a convex bending mode while compressive strain for a concave one. In a multicomponent system, the neutral plane position depends on the thicknesses ($t_i$) and the mechanical properties of the constituent layers (with Young´s modulus $E_i$). The general expression for a multilayer structure with $n$ components is[142]

$$\beta = \frac{\sum_{i=1}^{n} E_i t_i \left(\left(\sum_{j=1}^{n} t_j\right) - t_i/2\right)}{\sum_{i=1}^{n} E_i t_i} \tag{5}$$

In the case of a single oxide membrane supported on a thick flexible substrate ($t_s >> t_f$, where $t_s$ and $t_f$, are the thicknesses of the support and the film, respectively), the strain in the thin film can be approximated as:

$$\varepsilon_x = \frac{t_s}{2R} \tag{6}$$

Along the other directions (i.e., out of plane and perpendicular to the bending direction) a biaxial strain with opposite sign of $\varepsilon_x$ develop, proportional to the Poisson coefficient.[78] Figure 7e shows the expected strain in a supported-membrane as a function of the bending radius for different substrate thicknesses. One can note that larger strains are achievable by choosing thicker substrates but the ultimate strain will largely depends on the fracture point of the support, that is, the compressive and tensile strength.[93,142] For example, muscovite mica substrates, one of the most promising support for flexible electronics,[93]

can withstand a tensile strain up to ≈0.3% upon bending (for thickness between 15 and 85 μm).[143]

The mechanical bending strategy has been largely adopted for the study of the strain effect on transport and magnetic properties of perovskite membranes. Liu et al. found that the magnetic properties of SRO thin films deposited on muscovite mica are very sensitive to mechanical strain.[101] Upon bending, they observed a large variation of the Curie temperature, saturated magnetic moment, and coercive field. An increase of saturated moment from 1.2 to 3.2 $\mu$B per Ru was measured for a compression strain of −0.3% and was attributed to a spin state transition from low to high spin taking place under compressive in-plane strain. Li et al. also observed a significant effect of bending strain on the electrical resistivity of SRO thin films.[144] In their work, a decrease (increase) of resistivity of −26.05% (1.75%) was observed for a compressive strain of −0.25% (tensile, +0.25%). The decrease of resistivity upon compression originates from an increase of the Ru—O—Ru bond angle and by a rise of the density of state near the Fermi level, as probed by Raman and X-ray photoelectron spectroscopy. LSMO thin films are also known to give rise to a variation of resistivity[106] and magnetization[145,146] upon mechanical bending. In particular, Yao et al. showed that outward bending in $LaMnO_3$ thin films generates a significant modification of the oxygen octahedra and Mn—O—Mn bonds, which induces a larger overlaps between the Mn and O orbitals and a significant enhancement of saturation magnetization (92%) and of Curie temperature (123–130 K).[146] Similarly, strain effects on the electrical resistivity have been reported also for other perovskites oxides such as $SrVO_3$ and $BaNb_{0.5}Ti_{0.5}O_3$.[103,105] It is also worth noting that bending strain may affect other functional properties of perovskite oxides thin films, such as the photoluminescence intensity of Pr-doped $Ba_{0.85}Ca_{0.15}Ti_{0.9}Zr_{0.1}O_3$ thin films.[147]

The opportunity of dynamically tuning of ferroelectric and dielectric properties in ferroelectric supported thin films through mechanical bending was demonstrated by Ko et al.[143] In their work, the authors showed that BTO thin films on Mica substrates undergo a transformation from ferroelectric tetragonal to paraelectric cubic structure for both inward and outward bending mode, hindering the out of plane ferroelectric polarization. The results were used to build a mechanically controlled ferroelectric transistor, were the conductivity of the top electrode (Al-doped ZnO) can be modulated by the variation of ferroelectric polarization of the underlying BTO, controlled through the bending mechanism. Zhao et al. explored the multiferroic properties of (Fe)/BTO membranes on PDMS substrate during mechanical bending.[33] They found that the compressive strain enhances the ferromagnetic resonance of the Fe layer along the out-of-plane direction, due to a variation of the electric field at the Fe/BTO interface tuned by the rotation of ferroelectric domains.

Mechanical bending also introduces a strain gradient in the structure, equal to $\frac{d\epsilon}{d\beta} = 1/R$ (see [7]c). In perovskite oxides, strain gradients can give rise to the generation of electric fields, through the flexoelectric effect.[48] Guo et al. showed that ferroelectric $BiFeO_3$ membranes on PDMS withstand significant strain gradients during the mechanical bending, which can be used to modulate the photovoltage and photocurrent generated in the layers.[48] Jiang et al. also show the flexoelectric control of the photoconductivity in $LaFeO_3/LaNiO_3$ heterostructures on muscovite mica, where a continuous change of short-circuit current density upon bending was reported.[148]

In the case of a self-standing membrane (Figure 7d), the position of the neutral plane will be equal to half its thickness ($b_i = t_f/2$, where $t_f$ is the thicknesses of the film) and the strain in the outer/inner surfaces can be written as: $\epsilon_x = t_f/2R$. Clearly, compared to the substrate supported membranes, the radius of curvature needs to be significant smaller for achieving similar strains, which can be accomplished by the use of nanomanipulators[35] or by other external stimuli[69] in scanning or transmission electron microcopies. As commented in Section 3.2, the study of ferroelectric self-sustained membranes subjected to large bending strain showed that these ceramic materials, generally considered brittle in bulk, possesses superelasticity and ultraflexibility at the nanoscale.[69,30,35,38,122] Dong et al. first showed that single-crystalline ferroelectric BTO membrane can withstand an remarkable tensile strain of 10% without breaking.[30] The origin of this superelasticity was found to lie in a continuous rotation of the polarization direction in BTO membranes, which efficiently avoid mismatch stress and delay the membrane failure. Peng et al. found also that multiferroic $BiFeO_3$ membranes displays superelasticity, due to a reversible rhombohedral–tetragonal phase transition taking place in the most strained regions.[35] Such superior flexibility can also be observed in periodic wrinkles that can be formed during the membranes releasing and transfer process.[122]

Overall, mechanical bending emerges as a reliable strategy to investigate strain effects on perovskite oxide membrane. The ability to actively control the strain state in the same sample by controlling the radius of curvature allows a systematic and precise study of the variation of functional properties. The limitations of this method for substrate-supported thin films mainly arise from the limited strain that can be imposed without affecting the mechanical properties of the support, while for self-standing membranes from the requirements of nanomanipulators needed to achieve large strain states.

### 4.3. Mechanical Stretching

Mechanical stretching of single-crystal perovskite membranes is emerging as a new fascinating strategy to study the functional properties of perovskite oxides under tensile strain. This technique is based on the deposition of single-crystal thin films on a sacrificial layer and the subsequent transfer of the membrane on a flexible polymer (see Section 2.1.2), such as PI[55,52] or PET.[25] The support can then be stretched in a biaxial or uniaxial mode by micro-manipulators (see Figure 7f,g, respectively), producing a tensile strain in the structure equal to $\epsilon_i = \Delta L/L_0$, where $\Delta L$ and $L_0$ are the elongation and the initial length, respectively.[149] The adhesion between the thick polymer and the nanometric membrane allows the transfer of the strain state from the support to the thin film. As commented in Section 3.3, it was shown that freestanding perovskite thin films can withstand extremely large tensile strain before breaking, allowing the investigation of strain states not achievable in bulk and substrate-supported perovskite oxides.[22,23,69,30,35,38,122]

The mechanical stretching method was first used by Hong et al. to study the magnetotransport properties of

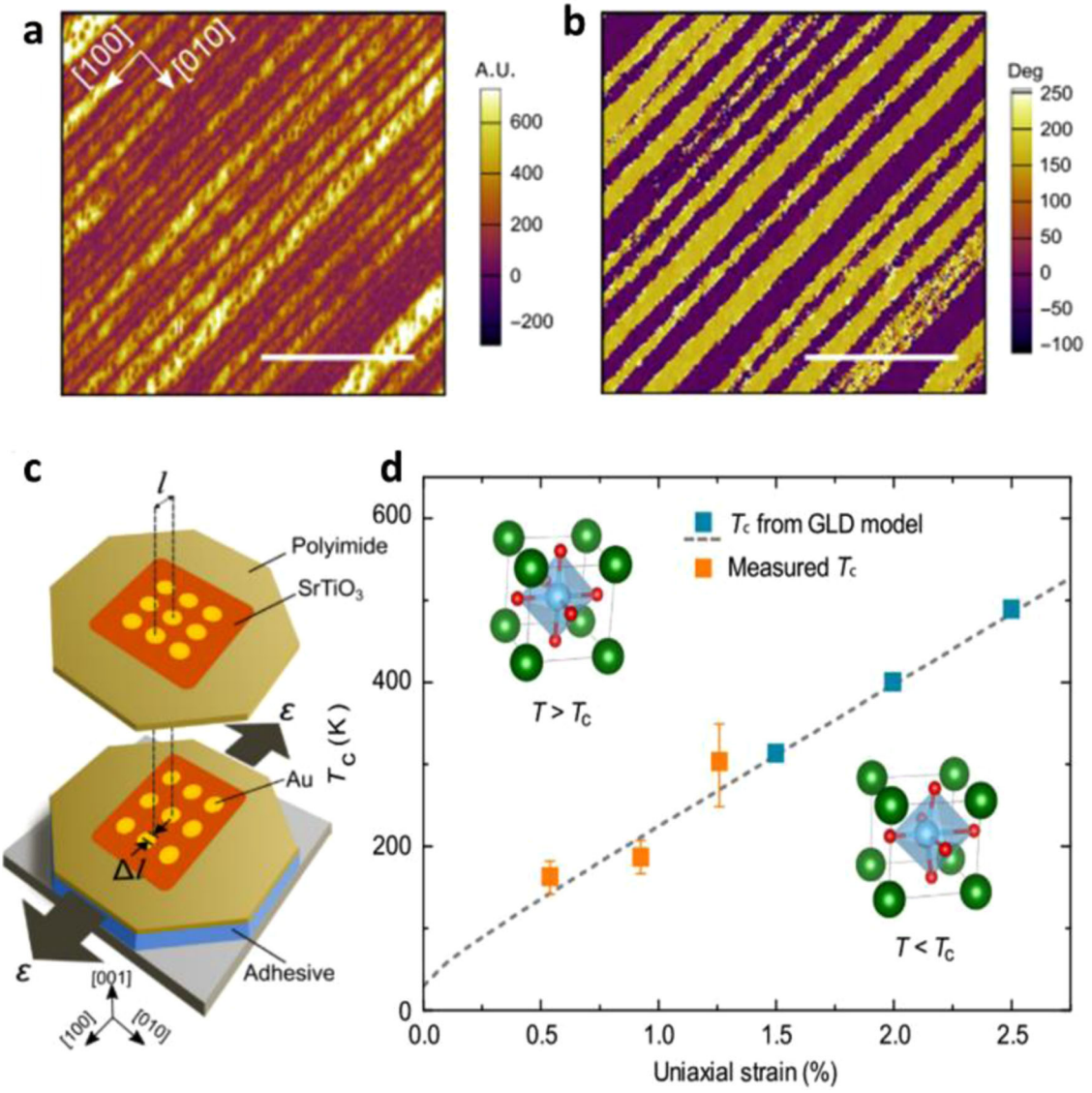


**Figure 8.** Strain-induced ferroelectricity in STO membranes. Piezoelectric force microscopy a) amplitude and b) phase measured for STO membranes under 2% uniaxial strain, showing the appearance of in-plane ferroelectric domains. c) Schematic of the uniaxial strain application on STO membranes. d) Ferroelectric transition temperature ($T_c$) measured in STO membranes as a function of uniaxial strain and predicted by numerical models. Reproduced under terms of the CC-BY license.[52] Copyright 2020, Springer Nature.

$La_{0.7}Ca_{0.3}MnO_3$ under extreme uniaxial and biaxial tensile strain (8% and 5%, respectively).[55] They found that strain promoted a transition from ferromagnetic metal to antiferromagnetic insulator, evidenced by orders of magnitude increase of resistivity at low temperature. The antiferromagnetic state is characterized by a charge/orbital ordering consisting in alternating Jahn–Teller-distorted $Mn^{3+}O_6$ octahedra and $Mn^{4+}O_6$, and can be quenched by the application of magnetic fields. Mechanical stretching was also employed for controlling the domain orientation in ferroelectric $PbTiO_3$ membranes and to induce room temperature ferroelectricity in STO membranes.[25,52] In particular, Xu et al. showed that tensile strain can linearly increase the ferroelectric transition temperature of STO, giving rise to the creation of in-plane polarized 180° domain structure aligned along the strain direction, see **Figure 8**.[52] The ability to manipulate the polarization direction through strain was also exploited by Zang et al. to engineer the interfacial thermal resistance in self standing Al/$BiFeO_3$ membranes.[51] In their work, the variation of polarization direction in ferroelectric $BiFeO_3$ through strain gave rise to a redistribution of the charge at the interface and eventually, through electron–phonon coupling, to a modification of the interface thermal resistance.

Overall, mechanical stretching appears as a promising method for tuning tensile strain of perovskite oxide membrane. The main advantage of this strategy is the possibility of controlling the strain state on the very same sample and the enormous strain that can be achieved. Nevertheless, due to the flexibility of the stretchable support, only tensile strain can be applied, which hinder the study of compressive strain states.

## 5. Outlook

Oxide-based freestanding membranes have the potentials to become the preferred candidates to next-generation oxide materials coupling the high selectivity to high functionality of these materials. However, it is not expected that the uptake of oxide-based freestanding membranes may occur in the short term, as novel fabrication, releasing and transferring processes needed to be further developed to take the full advantages of the oxides. Several approaches have been reported in this review paper for synthesizing, transferring, and measuring the freestanding oxide properties. What is still needed in the short term is the understanding of how to transfer large defect-free membrane size. Freestanding oxides show already unique properties and hence have significant potential for further new discoveries making them both interesting and challenging research subjects. Continuous development of operando probes and their combination as well as theoretical tools will help addressing the urgent questions regarding the relation between the freestanding oxide chemistry and their properties. Stacking, twisting, gate-modulating, and optically exciting have opened up a new field in 2D materials with promising ways in which unexpected strong correlations, topological, and symmetry-induced phenomena have been discovered. This, however, has never been tried before in oxide freestanding membranes and can lead to progress in synthesis, experimental tools, and potential new properties as well as applications of these materials. Finally, the rich science revealed so far in 2D moiré superlattice solids can be expected to remain an important source of stimulating scientific discoveries in freestanding oxide membranes. These directions could lead to new science, engineering, and application discoveries in atomically designed freestanding oxide materials.

## Acknowledgements

F.M.C., D.V.C., and N.P. acknowledge the funding from Villum Fonden for the NEED project (00027993). Y.L. acknowledges the support by the National Natural Science Foundation of China (Grant No. 11704292), and gratefully acknowledges financial support from China Scholarship Council (Grant No. 201908420153). F.T. acknowledges support by research grant 37338 (SANSIT) from Villum Fonden. N.P. acknowledges the funding from the Danish Council for Independent Research Technology and Production Sciences for the DFF Research Project 3 PILOT (Grant No. 00069B) and the Novo Nordisk Foundation "Challenge programme 2021 – Smart Nanomaterials for Applications in Life-Science" BIO-MAG (Grant No. NNF21OC0066526).

## Conflict of Interest

The authors declare no conflict of interest.

## Keywords

freestanding thin films, lattice strain, perovskite oxides, sacrificial layers, ultrathin membranes

Received: February 28, 2022
Revised: May 9, 2022
Published online: June 14, 2022

[1] R. P. Feynman, *Eng. Sci.* **1960**, *23*, 22.
[2] A. Chaves, J. G. Azadani, H. Alsalman, D. R. da Costa, R. Frisenda, A. J. Chaves, S. H. Song, Y. D. Kim, D. He, J. Zhou, A. Castellanos-Gomez, F. M. Peeters, Z. Liu, C. L. Hinkle, S. H. Oh, P. D. Ye, S. J. Koester, Y. H. Lee, P. Avouris, X. Wang, T. Low, *npj 2D Mater. Appl.* **2020**, *4*, 29.
[3] M. Zeng, Y. Xiao, J. Liu, K. Yang, L. Fu, *Chem. Rev.* **2018**, *118*, 6236.
[4] K. T. Faber, T. Asefa, M. Backhaus-Ricoult, R. Brow, J. Y. Chan, S. Dillon, W. G. Fahrenholtz, M. W. Finnis, J. E. Garay, R. E. García, Y. Gogotsi, S. M. Haile, J. Halloran, J. Hu, L. Huang, S. D. Jacobsen, E. Lara-Curzio, J. LeBeau, W. E. Lee, C. G. Levi, I. Levin, J. A. Lewis, D. M. Lipkin, K. Lu, J. Luo, J. P. Maria, L. W. Martin, S. Martin, G. Messing, A. Navrotsky, et al., *J. Am. Ceram. Soc.* **2017**, *100*, 1777.
[5] D. V. Christensen, F. Trier, W. Niu, Y. Gan, Y. Zhang, T. S. Jespersen, Y. Chen, N. Pryds, *Adv. Mater. Interfaces* **2019**, *6*, 1900772.
[6] A. Tarancón, N. Pryds, *Adv. Mater. Interfaces* **2019**, *6*, 1900990.
[7] M. Coll, J. Fontcuberta, M. Althammer, M. Bibes, H. Boschker, A. Calleja, G. Cheng, M. Cuoco, R. Dittmann, B. Dkhil, I. El Baggari, M. Fanciulli, I. Fina, E. Fortunato, C. Frontera, S. Fujita, V. Garcia, S. T. B. Goennenwein, C. G. Granqvist, J. Grollier, R. Gross, A. Hagfeldt, G. Herranz, K. Hono, E. Houwman, M. Huijben, A. Kalaboukhov, D. J. Keeble, G. Koster, L. F. Kourkoutis, et al., *Appl. Surf. Sci.* **2019**, *482*, 1.
[8] S. A. Chambers, *Surf. Sci.* **2011**, *605*, 1133.
[9] M. Bruel, *Nucl. Instrum. Methods Phys. Res., Sect. B* **1996**, *108*, 313.
[10] W. S. Wong, T. Sands, N. W. Cheung, *Appl. Phys. Lett.* **1998**, *72*, 599.
[11] D. Ji, S. Cai, T. R. Paudel, H. Sun, C. Zhang, L. Han, Y. Wei, Y. Zang, M. Gu, Y. Zhang, W. Gao, H. Huyan, W. Guo, D. Wu, Z. Gu, E. Y. Tsymbal, P. Wang, Y. Nie, X. Pan, *Nature* **2019**, *570*, 87.
[12] D. Lu, D. J. Baek, S. S. Hong, L. F. Kourkoutis, Y. Hikita, H. Y. Hwang, *Nat. Mater.* **2016**, *15*, 1255.
[13] D. Lu, S. Crossley, R. Xu, Y. Hikita, H. Y. Hwang, *Nano Lett.* **2019**, *19*, 3999.
[14] H. S. Kum, H. Lee, S. Kim, S. Lindemann, W. Kong, K. Qiao, P. Chen, J. Irwin, J. H. Lee, S. Xie, S. Subramanian, J. Shim, S. H. Bae, C. Choi, L. Ranno, S. Seo, S. Lee, J. Bauer, H. Li, K. Lee, J. A. Robinson, C. A. Ross, D. G. Schlom, M. S. Rzchowski, C. B. Eom, J. Kim, *Nature* **2020**, *578*, 75.
[15] A. Sambri, M. Scuderi, A. Guarino, E. Di Gennaro, R. Erlandsen, R. T. Dahm, A. V. Bjørlig, D. V. Christensen, R. Di Capua, B. D. Ventura, U. S. di Uccio, S. Mirabella, G. Nicotra, C. Spinella, T. S. Jespersen, F. M. Granozio, *Adv. Funct. Mater.* **2020**, *30*, 1909964.
[16] R. T. Dahm, R. Erlandsen, F. Trier, A. Sambri, E. Di Gennaro, A. Guarino, L. Stampfer, D. V. Christensen, F. M. Granozio, T. S. Jespersen, *ACS Appl. Mater. Interfaces* **2021**, *13*, 12341.
[17] S. J. Skinner, J. A. Kilner, *Mater. Today* **2003**, *6*, 30.
[18] Y. Zhang, C. Ma, X. Lu, M. Liu, *Mater. Horiz.* **2019**, *6*, 911.
[19] D. J. Baek, D. Lu, Y. Hikita, H. Y. Hwang, L. F. Kourkoutis, *ACS Appl. Mater. Interfaces* **2017**, *9*, 54.
[20] S. S. Hong, J. H. Yu, D. Lu, A. F. Marshall, Y. Hikita, Y. Cui, H. Y. Hwang, *Sci. Adv.* **2017**, *3*, eaao5173.
[21] D. Davidovikj, D. J. Groenendijk, A. M. R. V. L. Monteiro, A. Dijkhoff, D. Afanasiev, M. Šiškins, M. Lee, Y. Huang, E. van Heumen, H. S. J. van der Zant, A. D. Caviglia, P. G. Steeneken, *Commun. Phys.* **2020**, *3*, 163.
[22] V. Harbola, R. Xu, S. Crossley, P. Singh, H. Y. Hwang, *Appl. Phys. Lett.* **2021**, *119*, 053102.
[23] V. Harbola, S. Crossley, S. S. Hong, D. Lu, Y. A. Birkhölzer, Y. Hikita, H. Y. Hwang, *Nano Lett.* **2021**, *21*, 2470.
[24] J. A. Alonso, I. Rasines, J. L. Soubeyroux, *Inorg. Chem.* **1990**, *29*, 4768.
[25] L. Han, Y. Fang, Y. Zhao, Y. Zang, Z. Gu, Y. Nie, X. Pan, *Adv. Mater. Interfaces* **2020**, *7*, 1901604.

[26] S. Cai, Y. Lun, D. Ji, L. Han, C. Guo, Y. Zang, S. Gao, Y. Wei, M. Gu, C. Zhang, Z. Gu, X. Wang, C. Addiego, D. Fang, Y. Nie, J. Hong, P. Wang, X. Pan, **2020**, arXiv:2009.03177.
[27] P. T. P. Le, J. E. ten Elshof, G. Koster, *Sci. Rep.* **2021**, *11*, 12435.
[28] Z. Lu, J. Liu, J. Feng, X. Zheng, L. H. Yang, C. Ge, K. J. Jin, Z. Wang, R. W. Li, *APL Mater.* **2020**, *8*, 051105.
[29] H. Wang, L. Shen, T. Duan, C. Ma, C. Cao, C. Jiang, X. Lu, H. Sun, M. Liu, *ACS Appl. Mater. Interfaces* **2019**, *11*, 22677.
[30] G. Dong, S. Li, M. Yao, Z. Zhou, Y. Q. Zhang, X. Han, Z. Luo, J. Yao, B. Peng, Z. Hu, H. Huang, T. Jia, J. Li, W. Ren, Z. G. Ye, X. Ding, J. Sun, C. W. Nan, L. Q. Chen, J. Li, M. Liu, *Science* **2019**, *366*, 475.
[31] K. Gu, T. Katayama, S. Yasui, A. Chikamatsu, S. Yasuhara, M. Itoh, T. Hasegawa, *Adv. Funct. Mater.* **2020**, *30*, 2001236.
[32] R. Li, Y. Xu, J. Song, P. Wang, C. Li, D. Wu, *Appl. Phys. Lett.* **2020**, *116*, 222904.
[33] Y. Zhao, R. Peng, Y. Guo, Z. Liu, Y. Dong, S. Zhao, Y. Li, G. Dong, Y. Hu, J. Zhang, Y. Peng, T. Yang, B. Tian, Y. Zhao, Z. Zhou, Z. Jiang, Z. Luo, M. Liu, *Adv. Funct. Mater.* **2021**, *31*, 2009376.
[34] T. Wang, R. C. Peng, W. Peng, G. Dong, C. Zhou, S. Yang, Z. Zhou, M. Liu, *Adv. Funct. Mater.* **2021**, *32*, 2108496.
[35] B. Peng, R. C. Peng, Y. Q. Zhang, G. Dong, Z. Zhou, Y. Zhou, T. Li, Z. Liu, Z. Luo, S. Wang, Y. Xia, R. Qiu, X. Cheng, F. Xue, Z. Hu, W. Ren, Z. G. Ye, L. Q. Chen, Z. Shan, T. Min, M. Liu, *Sci. Adv.* **2020**, *6*, eaba5847.
[36] Z. Zhao, A. Abdelsamie, R. Guo, S. Shi, J. Zhao, W. Lin, K. Sun, J. Wang, J. Wang, X. Yan, J. Chen, *Nano Res.* **2021**, *15*, 2682.
[37] B. Wang, Y. Wu, X. Chen, Q. Han, Y. Chen, H. Wei, B. Cao, *Chem. Phys. Lett.* **2022**, *787*, 139207.
[38] C. Jin, Y. Zhu, X. Li, F. An, W. Han, Q. Liu, S. Hu, Y. Ji, Z. Xu, S. Hu, M. Ye, G. Zhong, M. Gu, L. Chen, *Adv. Sci.* **2021**, *8*, 2102178.
[39] S. Shrestha, M. Coile, M. Zhu, M. Souri, J. Kim, R. Pandey, J. W. Brill, J. Hwang, J. W. Kim, A. Seo, *ACS Appl. Nano Mater.* **2020**, *3*, 6310.
[40] F. An, K. Qu, G. Zhong, Y. Dong, W. Ming, M. Zi, Z. Liu, Y. Wang, B. Qi, Z. Ding, J. Xu, Z. Luo, X. Gao, S. Xie, P. Gao, J. Li, *Adv. Funct. Mater.* **2020**, *30*, 2003495.
[41] W. Hou, M. Yao, R. Qiu, Z. Wang, Z. Zhou, K. Shi, J. Pan, M. Liu, J. Hu, *J. Alloys Compd.* **2021**, *887*, 161470.
[42] B. Zhang, C. Yun, J. L. MacManus-Driscoll, *Nano-Micro Lett.* **2021**, *13*, 39.
[43] J. Park, J. H. Shin, K. Song, Y. J. Kim, H. B. Jang, H. Lee, H. S. Sim, C. H. Yang, *Appl. Phys. Lett.* **2020**, *116*, 022401.
[44] D. J. Baek, D. Lu, Y. Hikita, H. Y. Hwang, L. F. Kourkoutis, *APL Mater.* **2017**, *5*, 096108.
[45] Z. D. Luo, J. J. P. Peters, A. M. Sanchez, M. Alexe, *ACS Appl. Mater. Interfaces* **2019**, *11*, 23313.
[46] Z. Chen, B. Y. Wang, B. H. Goodge, D. Lu, S. S. Hong, D. Li, L. F. Kourkoutis, Y. Hikita, H. Y. Hwang, *Phys. Rev. Mater.* **2019**, *3*, 060801(R).
[47] C. Jin, Y. Zhu, W. Han, Q. Liu, S. Hu, Y. Ji, Z. Xu, S. Hu, M. Ye, L. Chen, *Appl. Phys. Lett.* **2020**, *117*, 252902.
[48] R. Guo, L. You, W. Lin, A. Abdelsamie, X. Shu, G. Zhou, S. Chen, L. Liu, X. Yan, J. Wang, J. Chen, *Nat. Commun.* **2020**, *11*, 2571.
[49] G. Zhong, F. An, K. Qu, Y. Dong, Z. Yang, L. Dai, S. Xie, R. Huang, Z. Luo, J. Li, *Small* **2022**, *18*, 2104213.
[50] H. Y. Sun, C. C. Zhang, J. M. Song, J. H. Gu, T. W. Zhang, Y. P. Zang, Y. F. Li, Z. B. Gu, P. Wang, Y. F. Nie, *Thin Solid Films* **2020**, *697*, 137815.
[51] Y. Zang, C. Di, Z. Geng, X. Yan, D. Ji, N. Zheng, X. Jiang, H. Fu, J. Wang, W. Guo, H. Sun, L. Han, Y. Zhou, Z. Gu, D. Kong, H. Aramberri, C. Cazorla, J. Íñiguez, R. Rurali, L. Chen, J. Zhou, D. Wu, M. Lu, Y. Nie, Y. Chen, X. Pan, *Adv. Mater.* **2021**, *34*, 2105778.
[52] R. Xu, J. Huang, E. S. Barnard, S. S. Hong, P. Singh, E. K. Wong, T. Jansen, V. Harbola, J. Xiao, B. Y. Wang, S. Crossley, D. Lu, S. Liu, H. Y. Hwang, *Nat. Commun.* **2020**, *11*, 3141.
[53] Y.-T. Shao, S. Das, Z. Hong, R. Xu, S. Chandrika, F. Gómez-Ortiz, P. García-Fernández, L.-Q. Chen, H. Hwang, J. Junquera, L. Martin, R. Ramesh, D. Muller, *Microsc. Microanal.* **2021**, *27*, 348.
[54] Z. Lu, Y. Yang, L. Wen, J. Feng, B. Lao, X. Zheng, S. Li, K. Zhao, B. Cao, Z. Ren, D. Song, H. Du, Y. Guo, Z. Zhong, X. Hao, Z. Wang, R.-W. Li, *npj Flexible Electron.* **2021**, *6*, 9.
[55] S. S. Hong, M. Gu, M. Verma, V. Harbola, B. Y. Wang, D. Lu, A. Vailionis, Y. Hikita, R. Pentcheva, J. M. Rondinelli, H. Y. Hwang, *Science* **2020**, *368*, 71.
[56] P. Singh, A. Swartz, D. Lu, S. S. Hong, K. Lee, A. F. Marshall, K. Nishio, Y. Hikita, H. Y. Hwang, *ACS Appl. Electron. Mater.* **2019**, *1*, 1269.
[57] A. K. Prodjosantoso, B. J. Kennedy, B. A. Hunter, *Aust. J. Chem.* **2000**, *53*, 195.
[58] D. Li, C. Adamo, B. Y. Wang, H. Yoon, Z. Chen, S. S. Hong, D. Lu, Y. Cui, Y. Hikita, H. Y. Hwang, *Nano Lett.* **2021**, *21*, 4454.
[59] J. W. Bullard, H. M. Jennings, R. A. Livingston, A. Nonat, G. W. Scherer, J. S. Schweitzer, K. L. Scrivener, J. J. Thomas, *Cem. Concr. Res.* **2011**, *41*, 1208.
[60] J. Shin, V. B. Nascimento, G. Geneste, J. Rundgren, E. W. Plummer, B. Dkhil, S. V. Kalinin, A. P. Baddorf, *Nano Lett.* **2009**, *9*, 3720.
[61] X. Li, Y. Bai, B. C. Wang, Y. J. Su, *J. Appl. Phys.* **2015**, *118*, 094104.
[62] S. R. Bakaul, C. R. Serrao, M. Lee, C. W. Yeung, A. Sarker, S. L. Hsu, A. K. Yadav, L. Dedon, L. You, A. I. Khan, J. D. Clarkson, C. Hu, R. Ramesh, S. Salahuddin, *Nat. Commun.* **2016**, *7*, 10547.
[63] S. R. Bakaul, C. R. Serrao, O. Lee, Z. Lu, A. Yadav, C. Carraro, R. Maboudian, R. Ramesh, S. Salahuddin, *Adv. Mater.* **2017**, *29*, 1605699.
[64] S. R. Bakaul, J. Kim, S. Hong, M. J. Cherukara, T. Zhou, L. Stan, C. R. Serrao, S. Salahuddin, A. K. Petford-Long, D. D. Fong, M. V. Holt, *Adv. Mater.* **2020**, *32*, 1907036.
[65] S. R. Bakaul, S. Prokhorenko, Q. Zhang, Y. Nahas, Y. Hu, A. Petford-Long, L. Bellaiche, N. Valanoor, *Adv. Mater.* **2021**, *33*, 2105432.
[66] S. R. Bakaul, *AIP Adv.* **2021**, *11*, 115310.
[67] D. Pesquera, E. Parsonnet, A. Qualls, R. Xu, A. J. Gubser, J. Kim, Y. Jiang, G. Velarde, Y. L. Huang, H. Y. Hwang, R. Ramesh, L. W. Martin, *Adv. Mater.* **2020**, *32*, 2003780.
[68] L. Shen, L. Wu, Q. Sheng, C. Ma, Y. Zhang, L. Lu, J. Ma, J. Ma, J. Bian, Y. Yang, A. Chen, X. Lu, M. Liu, H. Wang, C. L. Jia, *Adv. Mater.* **2017**, *29*, 1702411.
[69] H. Elangovan, M. Barzilay, S. Seremi, N. Cohen, Y. Jiang, L. W. Martin, Y. Ivry, *ACS Nano* **2020**, *14*, 5053.
[70] D. Pesquera, E. Khestanova, M. Ghidini, S. Zhang, A. P. Rooney, F. Maccherozzi, P. Riego, S. Farokhipoor, J. Kim, X. Moya, M. E. Vickers, N. A. Stelmashenko, S. J. Haigh, S. S. Dhesi, N. D. Mathur, *Nat. Commun.* **2020**, *11*, 3190.
[71] K. Eom, M. Yu, J. Seo, D. Yang, H. Lee, J. W. Lee, P. Irvin, S. H. Oh, J. Levy, C. B. Eom, *Sci. Adv.* **2021**, *7*, eabh1284.
[72] Y. Bourlier, B. Bérini, M. Frégnaux, A. Fouchet, D. Aureau, Y. Dumont, *ACS Appl. Mater. Interfaces* **2020**, *12*, 8466.
[73] N. Wiberg, E. Wiberg, A. Holleman, *Lehrbuch Der Anorganischen Chemie*, Walter de Gruyter GmbH & Co KG, location, Berlin **1995**.
[74] Y. W. Chang, P. C. Wu, J. B. Yi, Y. C. Liu, Y. Chou, Y. C. Chou, J. C. Yang, *Nanoscale Res. Lett.* **2020**, *15*, 172.
[75] C. C. Chiu, Y. W. Chang, Y. C. Shao, Y. C. Liu, J. M. Lee, S. W. Huang, W. Yang, J. Guo, F. M. F. de Groot, J. C. Yang, Y. De Chuang, *Sci. Rep.* **2021**, *11*, 5250.
[76] H. Peng, N. Lu, S. Yang, Y. Lyu, Z. Liu, Y. Bu, S. Shen, M. Li, Z. Li, L. Gao, S. Lu, M. Wang, H. Cao, H. Zhou, P. Gao, H. Chen, P. Yu, *Adv. Funct. Mater.* **2022**, https://doi.org/10.1002/adfm.202111907
[77] R. Takahashi, M. Lippmaa, *ACS Appl. Mater. Interfaces* **2020**, *12*, 25042.
[78] Y. Zhang, L. Shen, M. Liu, X. Li, X. Lu, L. Lu, C. Ma, C. You, A. Chen, C. Huang, L. Chen, M. Alexe, C. L. Jia, *ACS Nano* **2017**, *11*, 8002.

[79] D. Weber, R. Vofély, Y. Chen, Y. Mourzina, U. Poppe, *Thin Solid Films* **2013**, *533*, 43.
[80] X. Li, Z. Yin, X. Zhang, Y. Wang, D. Wang, M. Gao, J. Meng, J. Wu, J. You, *Adv. Mater. Technol.* **2019**, *4*, 1800695.
[81] D. K. Lee, Y. Park, H. Sim, J. Park, Y. Kim, G. Y. Kim, C. B. Eom, S. Y. Choi, J. Son, *Nat. Commun.* **2021**, *12*, 5019.
[82] Q. Wang, H. Fang, D. Wang, J. Wang, N. Zhang, B. He, W. Lü, *Crystals* **2020**, *10*, 733.
[83] J. Kang, D. Shin, S. Bae, B. H. Hong, *Nanoscale* **2012**, *4*, 5527.
[84] J. W. Suk, A. Kitt, C. W. Magnuson, Y. Hao, S. Ahmed, J. An, A. K. Swan, B. B. Goldberg, R. S. Ruoff, *ACS Nano* **2011**, *5*, 6916.
[85] F. Liu, W. Wu, Y. Bai, S. H. Chae, Q. Li, J. Wang, J. Hone, X. Y. Zhu, *Science* **2020**, *367*, 903.
[86] M. Sharma, A. Singh, R. Singh, *ACS Appl. Nano Mater.* **2020**, *3*, 4445.
[87] Y. Qi, J. Kim, T. D. Nguyen, B. Lisko, P. K. Purohit, M. C. McAlpine, *Nano Lett.* **2011**, *11*, 1331.
[88] Y. Chen, X. L. Gong, J. G. Gai, *Adv. Sci.* **2016**, *3*, 1500343.
[89] M. Yao, Y. Cheng, Z. Zhou, M. Liu, *J. Mater. Chem. C* **2019**, *8*, 14.
[90] P. C. Wu, Y. H. Chu, *J. Mater. Chem. C* **2018**, *6*, 6102.
[91] Y. H. Chu, *npj Quantum Mater.* **2017**, *2*, 67.
[92] Y. Bitla, Y. H. Chu, *Nanoscale* **2020**, *12*, 18523.
[93] Y. Bitla, Y. H. Chu, *FlatChem* **2017**, *3*, 26.
[94] A. Koma, *J. Cryst. Growth* **1999**, *201*, 236.
[95] A. Koma, K. Yoshimura, *Surf. Sci.* **1986**, *174*, 556.
[96] A. Koma, K. Ueno, K. Saiki, *J. Cryst. Growth* **1991**, *111*, 1029.
[97] J. Y. Hwang, Y. M. Kim, K. H. Lee, H. Ohta, S. W. Kim, *Nano Lett.* **2017**, *17*, 6140.
[98] C. Zhang, S. Ding, K. Qiao, J. Li, Z. Li, Z. Yin, J. Sun, J. Wang, T. Zhao, F. Hu, B. Shen, *ACS Appl. Mater. Interfaces* **2021**, *13*, 28442.
[99] M. Zheng, X. Y. Li, H. Ni, X. M. Li, J. Gao, *J. Mater. Chem. C* **2019**, *7*, 8310.
[100] L. Lu, Y. Dai, H. Du, M. Liu, J. Wu, Y. Zhang, Z. Liang, S. Raza, D. Wang, C. L. Jia, *Adv. Mater. Interfaces* **2020**, *7*, 1901265.
[101] J. Liu, Y. Feng, R. Tang, R. Zhao, J. Gao, D. Shi, H. Yang, *Adv. Electron. Mater.* **2018**, *4*, 1700522.
[102] J. Liu, S. Liu, Y. Wu, *J. Alloys Compd.* **2022**, *895*, 162725.
[103] R. Xu, X. Zhang, D. Zhang, J. Liu, J. Lu, R. Zhao, Y. Ji, F. Qian, H. Wang, J. Fan, W. Li, H. Yang, *J. Alloys Compd.* **2022**, *890*, 161897.
[104] W. Hou, S. Zhao, T. Wang, M. Yao, W. Su, Z. Hu, Z. Zhou, M. Liu, *Appl. Surf. Sci.* **2021**, *563*, 150074.
[105] C. Yang, M. Guo, D. Gao, W. He, J. Feng, A. Zhang, Z. Fan, D. Chen, M. Zeng, S. Wu, J. Gao, C. F. Guo, G. Zhou, X. Lu, J. Liu, *Adv. Mater. Technol.* **2019**, *4*, 1900578.
[106] M. Guo, C. Yang, D. Gao, Q. Li, A. Zhang, J. Feng, H. Yang, R. Tao, Z. Fan, M. Zeng, G. Zhou, X. Lu, J. M. Liu, *J. Mater. Sci. Technol.* **2020**, *44*, 42.
[107] Y. Yang, G. Yuan, Z. Yan, Y. Wang, X. Lu, J. M. Liu, *Adv. Mater.* **2017**, *29*, 1700425.
[108] D. L. Ko, T. Hsin, Y. H. Lai, S. Z. Ho, Y. Zheng, R. Huang, H. Pan, Y. C. Chen, Y. H. Chu, *Nano Energy* **2021**, *87*, 106149.
[109] S. A. Lee, J. Y. Hwang, E. S. Km, S. W. Kim, W. S. Choi, *ACS Appl. Mater. Interfaces* **2017**, *9*, 3246.
[110] J. J. Schermer, P. Mulder, G. J. Bauhuis, M. M. A. J. Voncken, J. Van Deelen, E. Haverkamp, P. K. Larsen, *Phys. Status Solidi A* **2005**, *202*, 501.
[111] J. W. Hutchinson, Z. Suo, *Adv. Appl. Mech.* **1991**, *29*, 63.
[112] F. Dross, J. Robbelein, B. Vandevelde, E. Van Kerschaver, I. Gordon, G. Beaucarne, J. Poortmans, *Appl. Phys. A: Mater. Sci. Process.* **2007**, *89*, 149.
[113] S. W. Bedell, K. Fogel, P. Lauro, D. Shahrjerdi, J. A. Ott, D. Sadana, *J. Phys. D: Appl. Phys.* **2013**, *46*, 152002.
[114] S. W. Bedell, P. Lauro, J. A. Ott, K. Fogel, D. K. Sadana, *J. Appl. Phys.* **2017**, *122*, 025103.
[115] D. Shahrjerdi, S. W. Bedell, *Nano Lett.* **2013**, *13*, 315.
[116] N. Li, S. Bedell, H. Hu, S. J. Han, X. H. Liu, K. Saenger, D. Sadana, *Adv. Mater.* **2017**, *29*, 1606638.
[117] S. W. Bedell, D. Shahrjerdi, B. Hekmatshoar, K. Fogel, P. A. Lauro, J. A. Ott, N. Sosa, D. Sadana, *IEEE J. Photovoltaics* **2012**, *2*, 141.
[118] D. Lebeugle, D. Colson, A. Forget, M. Viret, *Appl. Phys. Lett.* **2007**, *91*, 022907.
[119] C. C. Chiu, S. Z. Ho, J. M. Lee, Y. C. Shao, Y. Shen, Y. C. Liu, Y. W. Chang, Y. Z. Zheng, R. Huang, C. F. Chang, C. Y. Kuo, C. G. Duan, S. W. Huang, J. C. Yang, Y. De Chuang, *Nano Lett.* **2022**, *22*, 1580.
[120] Q. Lu, Z. Liu, Q. Yang, H. Cao, P. Balakrishnan, Q. Wang, L. Cheng, Y. Lu, J.-M. Zuo, H. Zhou, P. Quarterman, S. Muramoto, A. J. Grutter, H. Chen, X. Zhai, *ACS Nano* **2022**, *16*, 7580.
[121] P. Gumbsch, S. Taeri-Baghbadrani, D. Brunner, W. Sigle, M. Rühle, *Phys. Rev. Lett.* **2001**, *87*, 085505.
[122] G. Dong, S. Li, T. Li, H. Wu, T. Nan, X. Wang, H. Liu, Y. Cheng, Y. Zhou, W. Qu, Y. Zhao, B. Peng, Z. Wang, Z. Hu, Z. Luo, W. Ren, S. J. Pennycook, J. Li, J. Sun, Z. G. Ye, Z. Jiang, Z. Zhou, X. Ding, T. Min, M. Liu, *Adv. Mater.* **2020**, *32*, 2004477.
[123] V. Nagarajan, A. Roytburd, A. Stanishevsky, S. Prasertchoung, T. Zhao, L. Chen, J. Melngailis, O. Auciello, R. Ramesh, *Nat. Mater.* **2003**, *2*, 43.
[124] Q. Zhang, L. Xie, G. Liu, S. Prokhorenko, Y. Nahas, X. Pan, L. Bellaiche, A. Gruverman, N. Valanoor, *Adv. Mater.* **2017**, *29*, 1702375.
[125] S. Das, Y. L. Tang, Z. Hong, M. A. P. Gonçalves, M. R. McCarter, C. Klewe, K. X. Nguyen, F. Gómez-Ortiz, P. Shafer, E. Arenholz, V. A. Stoica, S. L. Hsu, B. Wang, C. Ophus, J. F. Liu, C. T. Nelson, S. Saremi, B. Prasad, A. B. Mei, D. G. Schlom, J. Íñiguez, P. García-Fernández, D. A. Muller, L. Q. Chen, J. Junquera, L. W. Martin, R. Ramesh, *Nature* **2019**, *568*, 368.
[126] Y. Li, E. Zatterin, M. Conroy, A. Pylypets, F. Borodavka, D. J. Groenendijk, E. Lesne, A. J. Clancy, M. Hadjimichael, Q. Ramasse, A. Caviglia, J. Hlinka, U. Bangert, S. Leake, P. Zubko, *Adv. Mater.* **2022**, *34*, 2106826.
[127] D. M. Juraschek, P. Narang, *Nano Lett.* **2021**, *21*, 5098.
[128] E. B. Guedes, T. W. Jensen, M. Naamneh, A. Chikina, R. T. Dahm, S. Yun, F. M. Chiabrera, N. C. Plumb, J. H. Dil, M. Shi, D. V. Christensen, W. H. Brito, N. Pryds, M. Radović, *J. Vac. Sci. Technol., A* **2022**, *40*, 013213.
[129] J. M. Rondinelli, N. A. Spaldin, *Adv. Mater.* **2011**, *23*, 3363.
[130] D. Sando, *J. Phys.: Condens. Matter* **2022**, *34*, 153001.
[131] J. Hwang, Z. Feng, N. Charles, X. R. Wang, D. Lee, K. A. Stoerzinger, S. Muy, R. R. Rao, D. Lee, R. Jacobs, D. Morgan, Y. Shao-Horn, *Mater. Today* **2019**, *31*, 100.
[132] A. Biswas, Y. H. Jeong, in *Epitaxy* (Ed: M. Zhong), Intech Open, London **2018**.
[133] A. D. Caviglia, R. Scherwitzl, P. Popovich, W. Hu, H. Bromberger, R. Singla, M. Mitrano, M. C. Hoffmann, S. Kaiser, P. Zubko, S. Gariglio, J. M. Triscone, M. Först, A. Cavalleri, *Phys. Rev. Lett.* **2012**, *108*, 136801.
[134] A. Fluri, C. W. Schneider, D. Pergolesi, *In Situ Stress Measurements of Metal Oxide Thin Films*, Elsevier Inc., New York **2018**.
[135] L. Qiao, K. H. L. Zhang, M. E. Bowden, T. Varga, V. Shutthanandan, R. Colby, Y. Du, B. Kabius, P. V. Sushko, M. D. Biegalski, S. A. Chambers, *Adv. Funct. Mater.* **2013**, *23*, 2953.
[136] J. R. Petrie, H. Jeen, S. C. Barron, T. L. Meyer, H. N. Lee, *J. Am. Chem. Soc.* **2016**, *138*, 7252.
[137] T. Mayeshiba, D. Morgan, *Solid State Ionics* **2017**, *311*, 105.
[138] F. Gunkel, D. V. Christensen, Y. Z. Chen, N. Pryds, *Appl. Phys. Lett.* **2020**, *116*, 120505.
[139] A. Fluri, D. Pergolesi, V. Roddatis, A. Wokaun, T. Lippert, *Nat. Commun.* **2016**, *7*, 10692.
[140] P. M. Mooney, G. M. Cohen, J. O. Chu, C. E. Murray, *Appl. Phys. Lett.* **2004**, *84*, 1093.

[141] X. Chen, W. Mi, *J. Mater. Chem. C* **2021**, *9*, 9400.
[142] L. Mao, Q. Meng, A. Ahmad, Z. Wei, *Adv. Energy Mater.* **2017**, *7*, 1700535.
[143] D. L. Ko, M. F. Tsai, J. W. Chen, P. W. Shao, Y. Z. Tan, J. J. Wang, S. Z. Ho, Y. H. Lai, Y. L. Chueh, Y. C. Chen, D. P. Tsai, L. Q. Chen, Y. H. Chu, *Sci. Adv.* **2020**, *6*, eaaz3180.
[144] Y. Li, P. Zhou, Y. Qi, T. Zhang, *J. Am. Ceram. Soc.* **2021**, *105*, 2038.
[145] J. Huang, H. H. Wang, X. Sun, X. Zhang, H. H. Wang, *ACS Appl. Mater. Interfaces* **2018**, *10*, 42698.
[146] H. Yao, K. Jin, Z. Yang, Q. Zhang, W. Ren, S. Xu, M. Yang, L. Gu, E. J. Guo, C. Ge, C. Wang, X. Xu, D. Zhang, G. Yang, *Adv. Mater. Interfaces* **2021**, *8*, 2101499.
[147] M. Zheng, H. Sun, K. W. Kwok, *NPG Asia Mater* **2019**, *11*, 52.
[148] Z. Jiang, Z. Xu, Z. Xi, Y. Yang, M. Wu, Y. Li, X. Li, Q. Wang, C. Li, D. Wu, Z. Wen, *J. Mater.* **2021**, *8*, 281.
[149] C. W. Hicks, M. E. Barber, S. D. Edkins, D. O. Brodsky, A. P. Mackenzie, *Rev. Sci. Instrum.* **2014**, *85*, 065003.

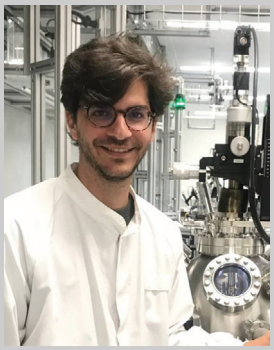

**Francesco Chiabrera** holds a M.Sc. in energy and nuclear engineering from the Polytechnic of Turin and a Ph.D. in nanoscience from the University of Barcelona. He has carried out Ph.D. research at the Catalonia Institute for Energy Research (IREC) in interface-dominated oxide thin films for energy storage and conversion. From 2020, he joined as postdoc in the group of Functional Oxide, Technical University of Denmark, where he is currently studying emerging functionalities in freestanding oxide thin-films for energy and information technology.

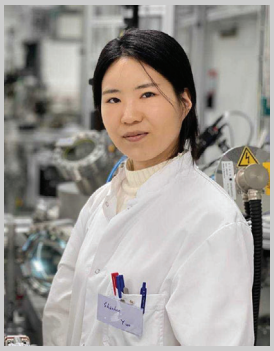

**Shinhee Yun** is currently working in the group of Functional Oxide (FOX) in the Department of Energy Conversion and Storage, the Technical University of Denmark as a postdoc. She was born in South Korea in 1989 and received a Ph.D. degree from the Department of Physics, Korea Advanced Institute of Science and Technology in 2020. In the same year, she joined FOX. Her research interests include flexoelectricity for sustainable energy and related functionalities as nanodevices.

**Thomas Sand Jespersen** received his Ph.D. in 2007 from the Niels Bohr Institute, University of Copenhagen, Denmark on the topics of scanning probe characterization and electron transport in nanoscale semiconductors. Since 2012 he is an associate professor at Niels Bohr Institute focusing on experimental studies of correlated phenomena in oxide heterostructures and quantum transport and developments of semiconductor/superconductor epitaxial hybrid nanomaterials. Since 2021, he is a professor at the Technical University of Denmark, Department of Energy.

**Nini Pryds** is professor and heading the research section 'Functional Oxide' at the Department of Energy Conversion and Storage, The Technical University of Denmark (DTU), where he is leading a group of 35+ researchers working in the field of complex oxide thin films for applications in a wide range of energy and information technologies. He made major contributions in emerging disciplines such as nanoionics and iontronics, dealing with the design and control of interface-related phenomena in fast ionic and electronic conductors. His main interest is aimed at exploring how broken symmetries at interfaces affect magnetic, electronic, and ionic properties.